Technical Report IRRP-96-4
March 1996

US Army Corps of Engineers
Waterways Experiment Station

Installation Restoration Research Program

Development of Laser-Induced Breakdown Spectroscopy for Detection of Metal Contaminants in Soils

by Javier Cortes, Ernesto R. Cespedes, Brian H. Miles

Prepared for Headquarters, U.S. Army Corps of Engineers

DISCLAIMER NOTICE

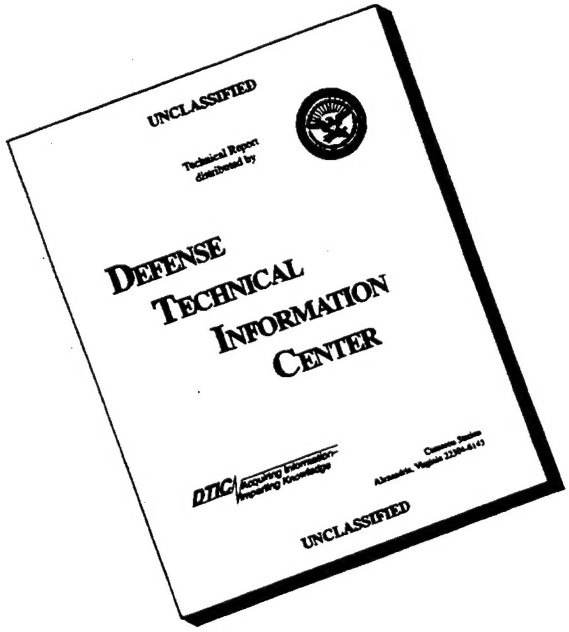

THIS DOCUMENT IS BEST QUALITY AVAILABLE. THE COPY FURNISHED TO DTIC CONTAINED A SIGNIFICANT NUMBER OF PAGES WHICH DO NOT REPRODUCE LEGIBLY.

PRINTED ON RECYCLED PAPER

Installation Restoration Research Program

Technical Report IRRP-96-4
March 1996

Development of Laser-Induced Breakdown Spectroscopy for Detection of Metal Contaminants in Soils

by Javier Cortes, Ernesto R. Cespedes, Brian H. Miles

U.S. Army Corps of Engineers
Waterways Experiment Station
3909 Halls Ferry Road
Vicksburg, MS 39180-6199

Final report

Approved for public release; distribution is unlimited

Prepared for U.S. Army Corps of Engineers
Washington, DC 20314-1000

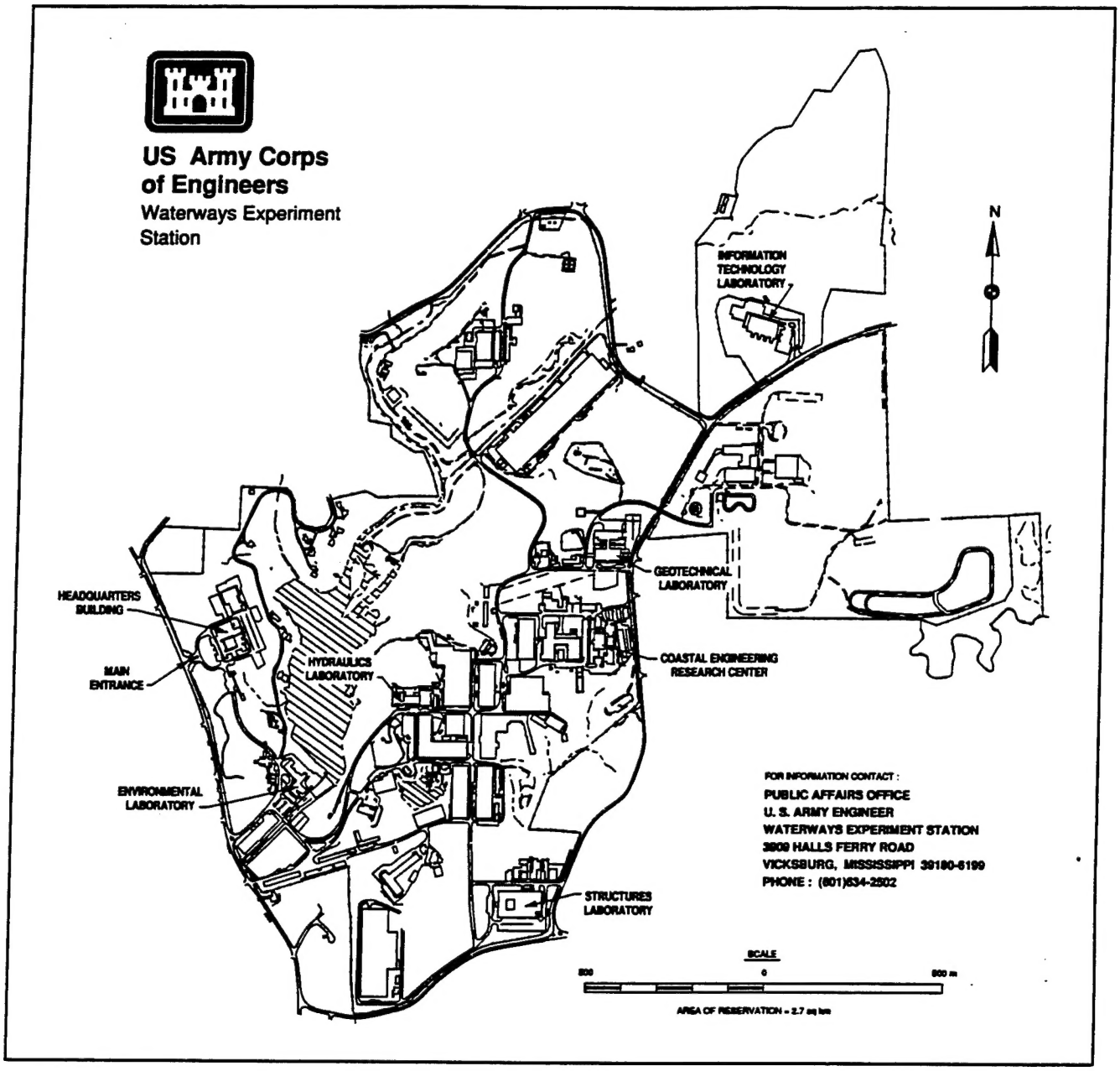

Waterways Experiment Station Cataloging-in-Publication Data

Cortes, Javier.

Development of laser-induced breakdown spectroscopy for detection of metal contaminants in soils / by Javier Cortes, Ernesto R. Cespedes, Brian H. Miles ; prepared for U.S. Army Corps of Engineers.

72 p. : ill. ; 28 cm. -- (Technical report ; IRRP-96-4)

Includes bibliographic references.

1. Soil pollution -- Environmental aspects. 2. Soil remediation -- Environmental aspects. 3. Heavy metals -- Environmental aspects -- Testing. 4. Spectroscopic imaging -- Environmental aspects -- Testing. I. Cespedes, Ernesto R. II. Miles, Brian H. III. United States. Army. Corps of Engineers. IV. U.S. Army Engineer Waterways Experiment Station. V. Installation Restoration Research Program. VI. Title. VII. Series: Technical report (U.S. Army Engineer Waterways Experiment Station) ; IRRP-96-4.

TA7 W34 no.IRRP-96-4

Contents

Preface vii

1—Introduction 1

2—LIBS Experimental Setup 4

Sample Preparation 4
Preparation of liquid samples for experiments 4
Preparation of soil samples for early LIBS experiments 5
Preparation of soil samples for detection-limit experiments (FY94) 6
Preparation of soil samples contaminated with mercury for detection-limit experiments 8
Hardware Setup 9
Basic setup 9
Liquid sample setup 10
Soil sample setup 10
Instrumentation 10

3—Experimental Considerations 13

Data Collection Controls 13
Resolution Issues 13
Energy Level Issues 16
Detector and Data Processing Issues 16

4—LIBS Data Collection 27

Early Experiments 27
Results of liquid sample experiments 27
Results of pure metals experiments 30
Results of soil sample experiments 31
Later Measurements 36

5—New Detection Limits 50

Peak Selection for Analysis of Data 50
Calculation of Spectral Areas 51
Results of Detection-Limit Calculation 53

6—Conclusions 67
References 71
SF 298

List of Figures

Figure 1. LIBS setup—liquid sample 11
Figure 2. LIBS setup—soil sample 12
Figure 3. Spectrum of Fisher sea sand using a 600-groove/mm grating 14
Figure 4. Spectrum of Fisher sea sand using a 2,400-groove/mm grating 14
Figure 5. Comparison of resolution between the 600- and 2,400-groove/mm grating 15
Figure 6. Overlap comparison of spectra using 600- and 2,400-groove/mm grating 15
Figure 7. Spectra of Yuma sand at laser energies of 125 and 85 mJ with 7.71 ppm of Pb 17
Figure 8. Spectra of Yuma sand at laser energies of 60, 45, and 30 mJ with 7.71 ppm of Pb 17
Figure 9. Collection of broad band emission and Yuma sand spectrum at gate delay of 64 ns and gate width of 100 μs . . . 19
Figure 10. Spectra of Yuma sand containing 132 ppm of lead at different gate delays and 100-μs gate width 21
Figure 11. Spectra of behavior of lead plasma from beginning of broad band emission until 300 ns 23
Figure 12. Plasma time evolution behavior from 300 to 700 ns 24
Figure 13. Plasma time evolution behavior from 700 to 1,500 ns 25
Figure 14. Plot of air lead plasma behavior at 100 mJ of laser energy . . 26
Figure 15. Calibration curve for Mn in water 28
Figure 16. Lower portion of calibration curve for Mn in water 29
Figure 17. Spectral plots of Mn in water 30
Figure 18. Superimposed spectra of lead in Yuma sand at approximated 100 and 500 ppm 33
Figure 19. Spectra of mercury from HgCl at different gate delays 36
Figure 20. Mercury spectra from HgCl at different gate delays 37

Figure 21. Behavior of 435.835-nm line of mercury in HgCl 37

Figure 22. Spectra of 435.835-nm line of mercury in Fisher sea sand at different Hg concentrations 39

Figure 23. Spectra of 253.652-nm line of mercury at 7,800 ppm in Yuma sand 41

Figure 24. Spectra of 296.652-nm line of mercury at 7,800 ppm in Yuma sand 41

Figure 25. Spectra of 365.015-nm line of mercury at 7,800 ppm in Yuma sand 43

Figure 26. Spectra of 404.656-nm line of mercury at 7,800 ppm in Yuma sand 43

Figure 27. Spectra of 435.835-nm line of mercury at 7,800 ppm in Yuma sand 45

Figure 28. Spectra of 546.074-nm line of mercury at 7,800 ppm in Yuma sand 45

Figure 29. Spectra from samples of DoD sites contaminated with lead and zinc (Fort Ord) 47

Figure 30. Spectra from samples of DoD sites contaminated with cadmium, lead, and zinc (Umatilla Army Depot) 48

Figure 31. Spectrum from a sample of a DoD site contaminated with mercury (Rocky Mountain Arsenal) 49

Figure 32. Spectra of 405.783-nm lead line in Yuma sand 52

Figure 33. Example of detection-limit analysis for Yuma sand contaminated with 108 ppm of lead 53

Figure 34. Calibration curve for detection-limit calculation of lead in Yuma sand at laser energy of 100 mJ 55

Figure 35. Calibration curve for detection-limit calculation of lead in Fisher sea sand at laser energy of 100 mJ 56

Figure 36. Calibration curve for detection-limit calculation of chromium in Fisher sea sand at laser energy of 100 mJ 57

Figure 37. Calibration curve for detection-limit calculation of cadmium in Fisher sea sand at laser energy of 100 mJ 58

Figure 38. Calibration curve for detection-limit calculation of mercury in Fisher sea sand at laser energy of 100 mJ 59

Figure 39. Calibration curve for detection-limit calculation of zinc in Fisher sea sand at laser energy of 100 mJ 60

Figure 40. Spectra of Yuma sand and 405.785-nm lead line at 7.71 and 22.4 ppm 61

Figure 41. Spectra of Fisher sea sand and 405.785-nm lead line at 1.53 and 2.00 ppm 61
Figure 42. Spectra of Fisher sea sand and 425.435-nm chromium line at 1.80 and 4.00 ppm 63
Figure 43. Spectra of Fisher sea sand and 214.438-nm cadmium line at 1.14 ppm 63
Figure 44. Spectra of Fisher sea sand and 435.835-nm mercury line at 17.2 ppm 65
Figure 45. Spectra of Fisher sea sand and 202.548-nm zinc line at 1.30 and 2.00 ppm 65
Figure 46. Preliminary results of quantification of LIBS data 69

List of Tables

Table 1. Preparation of 10,000-ppm Heavy Metal Solutions 5
Table 2. Heavy Metal Salts Used in LIBS Sample Preparation 7
Table 3. LIBS Mercury Samples 9
Table 4. Spectral Lines Observed in Pure Metal Experiments 31
Table 5. Results of Dry Soil Sample Test 35
Table 6. Summary of Spectral Lines Used for Detection Limits 51
Table 7. Summary of Detection Limits 60

Preface

The work reported herein was conducted by the Environmental Laboratory (EL) of the U.S. Army Engineer Waterways Experiment Station (WES). The research was sponsored by the Department of the Army Installation Restoration Research Program (IRRP), Environmental Quality and Technology Applied Research Work Unit entitled "Advanced Sensor Systems for the Cone Penetrometer System," Project AF25-CT-004, and by the Department of Energy's (DOE) Office of Technology Development. Dr. Clem Meyer was the IRRP Coordinator at the Directorate of Research and Development, Headquarters, U.S. Army Corps of Engineers. Dr. M. John Cullinane, WES, was the IRRP Program Manager. Dr. Carolyne Purdy was the DOE Program Manager.

The laboratory studies described in this report were designed and conducted by Messrs. Javier Cortes and Brian H. Miles, Environmental Sensing Branch (ESB), Environmental Engineering Division (EED), EL. Dr. Ernesto R. Cespedes, Chief, ESB, provided technical advice and assisted in the analysis of results and report preparation. The Environmental Chemistry Branch, EL, performed analyses of the soil and liquid samples used in this study.

The study was conducted under the general supervision of Mr. Norman R. Francingues, Chief, EED, and Dr. John W. Keeley, Director, EL.

At the time of publication of this report, Dr. Robert W. Whalin was Director of WES. COL Bruce K. Howard, EN, was the Commander.

This report should be cited as follows:

> Cortes, J., Cespedes, E. R., and Miles, B. H. (1996). "Development of laser-induced breakdown spectroscopy for detection of metal contaminants in soils," Technical Report IRRP-96-4, U.S. Army Engineer Waterways Experiment Station, Vicksburg, MS.

1 Introduction

Laser-induced breakdown spectroscopy (LIBS) involves optical techniques similar to flame, arc, spark, or inductively coupled plasma atomic emission spectrometry; all of these techniques are or have been used for the detection of metals. These techniques involve excitation of a plasma by high-temperature flame, high-voltage arcs, or high-electrical and magnetic fields. Some of these require that the metal be in a solution. In the case of soils, the material to be analyzed must be treated with an acid digestion in order to extract the metals for analysis. Once a sample solution is prepared, it is nebulized into a fine mist and sprayed into the excitation field where the solution is vaporized into a plasma (Fritz and Schenk 1987). The electrons of the atoms present in the plasma are excited into higher energy levels and some ions are generated. As the hot plasma cools, some electrons move from excited states to ground states by emitting photons of light. A sample of these photons are collected and analyzed by a spectrometer. The disadvantages of these excitation techniques are twofold. First, the sample often has to be in a solution. Second, the system is large and bulky.

The LIBS technique applied to subsurface analysis combines a laser, fiber optic cables, and spectrometer to make elemental analysis of soils in situ without removing a sample and preparing a solution. In LIBS, a high flux laser source is focused onto the sample of interest creating a plasma, and further ionization occurs through cascade ionization, in which the plasma front propagates toward the laser source, driven by absorption of the incidence pulse. Upon recombination of the plasma, the resulting photon emissions, occurring from the luminous region, will be characteristic of the ionized species present in the sample and surrounding gas (Alexander et al., In Preparation). The photon emission from the plasma is passed through a fiber optic to the spectrometer, where the emission data are collected and analyzed. The measured emission spectra of heavy metal contaminants display unique emission spectra and can be differentiated spectrally from nontoxic in situ materials. This characteristic makes LIBS a powerful screening tool for the real-time detection and analysis of soils contaminated with heavy metals.

Shortly after the discovery of the laser, it was noted that the breakdown of air could be caused by a focused laser beam (Weyl 1989). Subsequent investigations have focused on examining the spectroscopic properties of the laser

spark. Further studies began looking at the laser spark for use as a spectroscopic excitation tool; this technique is now called LIBS.

Laser-induced breakdown can be precipitated in two ways. The first is by cascade breakdown where an electron impacts a neutral atom with enough kinetic energy to ionize the atom, thereby ejecting an electron. This event will propagate exponentially with time. Requirements are that there be an initial electron in the focal volume and that the electron acquires energy exceeding the ionization energy of the material in the focus. The second way that breakdown can be started is by multiphoton ionization (MPI) where multiple photons interact with a single electron causing it to be ejected. Note that due to the inverse relationship between photon energy and wavelength, MPI is more improbable at longer laser wavelengths due to the increasing number of photons that would be required to free each electron.

For radiation at a wavelength of 1.064 μm, it is believed that the breakdown is predominated by cascade breakdown rather than MPI. The initial electron can be present due to previously ionized species or can be generated by MPI. The most likely scenario for the LIBS tests reported here is that the initial electron was produced by MPI, and the resulting breakdown was predominantly caused by cascade breakdown with a small contribution from MPI.

The strength of the spectral lines observed is due to the electron density present in the plasma, where the rate of change of electron density can be described as follows:

$$\frac{dn_e}{dt} = \nu_i n_e + W_m I^m n - \nu_a n_e - \nu_r n_e + \nabla \cdot (D \nabla n_e)$$

where

n_e = number of electrons per unit of volume

ν_i = impact ionization rate coefficient

W_m = multiphoton rate coefficient

I = intensity, W/cm^2

m = number of photons of a specified wavelength needed to ionize one atom

n = number of atoms per unit of volume

ν_a = attachment rate coefficient

ν_r = recombination rate coefficient

D = electron diffusion coefficient

The left term is the time rate of change of the number of electrons. The first additive term on the right represents electron generation due to impact ionization. The second additive term represents the MPI rate. The exponent on the intensity is the number of photons of a specified wavelength needed to ionize one electron of the material illuminated. For example, four 1.064-μm photons are needed to ionize one electron from lead. Multiphoton ionization rate coefficients are calculated based on several theoretical approximations or are determined by measurement at low gas densities. The third and fourth terms are negative and represent electron attachment and recombination. The fifth term represents the electron diffusion.

2 LIBS Experimental Setup

In 1992, the U.S. Army Engineer Waterways Experiment Station (WES) initiated an internally funded research program to determine the effectiveness of LIBS in detecting heavy metal contaminants in soil and groundwater and to evaluate its applicability as a Site Characterization and Analysis Penetrometer System (SCAPS) sensor. Throughout fiscal year 1993 (FY93), a number of experiments were conducted at WES and at the University of Nebraska in Lincoln (UNL) using Nd:YAG (1.064 μm) and KrF excimer (248 nm) laser-based systems to collect LIBS data on heavy metals in aqueous solutions and in three soil matrices (sand, silt, and clay).

WES provided soils and heavy metals solutions to UNL to perform a limited number of corroborating experiments for WES. Using those common samples, LIBS experiments were performed on contaminated liquid samples followed by pure metals, and by soil samples contaminated with heavy metals. The results of those experiments were the guidelines for the detection-limit experiments made in FY94.

Sample Preparation

Aqueous solutions of 10,000 ppm of cadmium, cobalt, chromium, copper, iron, manganese, nickel, molybdenum, lead, thallium, zinc, and mercury were prepared in WES's analytical laboratory for LIBS experiments (see Table 1). Those solutions were used in the preparation of contaminated liquid and soil samples.

Preparation of liquid samples for experiments

Liquid samples were prepared at different contamination levels for each metal. Contaminant concentrations ranging from 22 ppb to 1,500 ppm were achieved for each of the metals by the dilution of the acid 10,000-ppm metal solutions with deionized water.

Table 1
Preparation of 10,000-ppm Heavy Metal Solutions

Metal	Compound Used	Acid Solution
Cadmium	Cd	10% HNO_3
Cobalt	$CoCl_2 \cdot 6H_2O$	10% HNO_3
Chromium	$(NH_4)_2Cr_2O_7$	10% HNO_3
Copper	$CuSO_4 \cdot 5H_2O$	10% HNO_3
Iron	$FeCl_3 \cdot 6H_2O$	5% HNO_3
Manganese	$MnSO_4 \cdot H_2O$	10% HNO_3
Nickel	Ni	10% HNO_3
Molybdenum	$(NH_4)_2MoO_4$	10% HCl
Lead	$Pb(NO_3)_2$	10% HNO_3
Thallium	$Tl(NO_3)$	10% HNO_3
Zinc	Zn	10% HNO_3
Silver	$AgNO_3$	10% HNO_3
Mercury	$HgCl_2$	10% HCl

Preparation of soil samples for early LIBS experiments

Soil samples were prepared for three soil types (Arizona Yuma sand, Mississippi silt, and Mississippi clay) and at three moisture content levels: saturated, approximately 50-percent saturated, and dry using the 10,000-ppm acid solutions of lead, chromium, cadmium, mercury, and zinc. These five metals represent the highest priority contaminants in the investigations done in this report.

For each soil type, two samples, each having a volume of at least 1.5 times that of a petri dish sample holder (100-mm diam by 10-mm height), were placed in individual 250-ml beakers and weighed (approximated 150 g of soil). Deionized water was added to the pure sample until it was saturated. A volume of 10,000-ppm contaminant solution was then added to the other soil sample to equate moisture contents (the concentrations of the sample were in the range of 1,000 to 4,000 ppm). Both samples were weighed, and the moisture content and contaminant concentrations were calculated. The samples were then immediately stirred and placed in a covered petri dish for LIBS testing. After testing, the samples were returned to their respective beakers, and it was assumed that the moisture content was essentially unchanged during the testing (approximately 10 min). The beakers were weighed and placed in an oven. Approximately 2 hr of drying time at 100 °C was required to prepare medium moisture samples. The samples were taken from the oven and allowed to cool. The samples were then weighed to determine the moisture

content and placed in petri dishes. After LIBS testing, the samples were again returned to their beakers for weighing and final drying. The samples were allowed to dry at least 16 hr before being removed to prepare for dry sample tests. The samples were allowed to cool, and the dry, hard pieces were ground to near original consistency before being placed in petri dishes for final LIBS testing.

Another set of soil samples of Yuma sand, silt, and clay were prepared at 100- and 500-ppm contamination levels of lead, chromium, cadmium, mercury, and zinc. The samples were prepared by direct addition of 10,000-ppm acid solutions until the level of contamination to be tested was reached. Deionized water was added until the sample became oversaturated and then mixed to secure uniform concentration. Then the samples were dried in an oven at 100 °C for at least 24 hr. The calculation for these samples were made by mass concentration with a dry mass basis.

One problem in using acid solutions for preparation of the soil samples was that chemical reactions sometimes occurred when the solution was placed in contact with the soil. These reactions would change the soil matrix chemistry and affect the spectra collected. The contaminated samples displayed a smaller number of peaks than the uncontaminated soil's background. It was found that this technique of sample preparation was not adequate for the preparation of mercury samples. This prompted the investigation into a more suitable sample-preparation technique.

Preparation of soil samples for detection-limit experiments (FY94)

In FY93, the sample preparation was done in the three soils mentioned before. From those experiments, it was found easiest to detect contaminants in the Yuma sand, more difficult in silt, and most difficult in clay. Grain size and the density of the soil appear to have an effect on the plasma generation. The soils used in FY93 had a few parts-per-million natural content of lead, chromium, and zinc. This natural contamination interfered to some degree in the determination of detection limits of LIBS because there was a component of this metal's spectrum in the background.

An investigation of different sands, silts, and clays was conducted for the selection of one soil for a detection-limit concentration study. It was found that sea sand from a supply company by the name of Fisher contained the least number of contaminants and lowest concentration of each. Fisher sea sand was then selected for use in sample preparation for determining detection limits.

Research on sample preparation done in FY94 focused on how the contaminants were transported inside and through the soil. The principal transport is done by the pluvial precipitation, the groundwater flow, and leaching. Since the primary transport mechanism was by water, water-soluble salts of the heavy metals of interest were investigated and acid solutions were avoided.

The use of water-soluble salts also avoided the chemical reaction problem in soils that was alluded to earlier. The salts used were $Pb(NO_3)_2$, $CdNO_3 \cdot 5H_2O$, $ZnCl_2$, $K_2Cr_2O_7$, and $HgCl_2$ (see Table 2).

Table 2
Heavy Metal Salts Used in LIBS Sample Preparation

Heavy Metal Salt	Solvent	Soil	Background Concentration, ppm
$Pb(NO_3)_2$	deionized water	Yuma sand	7.71 Pb
$Pb(NO_3)_2$	deionized water	Fisher sea sand	1.53 Pb
$K_2Cr_2O_7$	deionized water	Fisher sea sand	1.80 Cr
$CdNO_3 \cdot 5H_2O$	deionized water	Fisher sea sand	<0.02 Cd
$HgCl_2$	acetone	Fisher sea sand	0.302 Hg
$ZnCl_2$	deionized water	Fisher sea sand	1.30 Zn

The new sample preparation consisted of the following procedure for all the metals except for mercury:

a. Weigh a small amount of the salt of the heavy metal of interest in a 250-ml beaker.

b. Add some water to dissolve it.

c. Weigh separately the corresponding amount of sand required to reach the concentration desired.

d. Add the soil to the solution and mix.

e. Add more water until all the soil is wet and a layer of water covers the soil and continue mixing.

f. Place the sample in an oven at 100 °C at least 24 hr.

Example of calculations performed to compute contaminant concentrations:

Pb atomic weight = 207.19 g/gmol
$Pb(NO_3)_2$ molecular weight = 331.21 g/gmol

Amount of $Pb(NO_3)_2$ used = 4.32 mg
Amount of sand used = 131,530 mg

$$ppm = \frac{\text{Pb mass} * 10^6}{\text{total mass}}$$

$$= \frac{Pb(NO_3)_2 \text{ used} * (\text{Pb atomic weight}/Pb(NO_3)_2 \text{ molecular weight}) * 10^6}{\text{Amount of } Pb(NO_3)_2 \text{ used} + \text{Amount of sand used}}$$

$$ppm = \frac{4.32 \text{ mg} * (207.19 \text{ g/gmol} / 331.21 \text{ g/gmol}) * 10^6}{4.32 \text{ mg} + 131{,}530 \text{ mg}}$$

ppm = 20 of Pb

All the calculations were made on a dry mass basis because it was assumed that all the water would leave the sample after being heated.

Preparation of soil samples contaminated with mercury for detection-limit experiments

This sample preparation consisted of using $HgCl_2$ and acetone as a solvent. The advantage of using acetone as a solvent is that it vaporized relatively quickly at ambient temperature. In addition, $HgCl_2$ is very soluble in acetone. The sample preparation procedure was as follows:

a. Weigh a small amount of $HgCl_2$ in a 250-ml beaker.

b. Add acetone and dissolve it.

c. Weigh separately the corresponding amount of sand required to reach a specific concentration.

d. Add the soil to the solution and mix.

e. Add more acetone until the soil is saturated and a layer of acetone covers the soil and continue mixing.

f. Let the acetone evaporate in a fume hood.

Example of calculations performed to compute contaminant concentrations:

Hg atomic weight = 200.59 g/gmol
$HgCl_2$ molecular weight = 271.50 g/gmol

Amount of $HgCl_2$ used = 4.91 mg
Amount of sand used = 151,211 mg

$$ppm = \frac{\text{Hg mass} * 10^6}{\text{total mass}}$$

$$= \frac{HgCl_2 \text{ used} * (\text{Hg atomic weight} / HgCl_2 \text{ molecular weight}) * 10^6}{\text{Amount of } HgCl_2 \text{ used} + \text{Amount of sand used}}$$

$$ppm = \frac{4.91 \text{ mg} * (200.59 \text{ g/gmol} / 271.50 \text{ g/gmol}) * 10^6}{4.91 \text{ mg} + 151{,}211 \text{ mg}}$$

ppm = 24 of Hg

The calculations were made on a dry mass basis because it was assumed that the solvent would leave the sample upon evaporation. All the samples were sent to the analytical laboratory at WES for certification of concentration. Certification techniques used were inductively coupled plasma atomic emission spectrometry and heated graphite furnace atomic absorption spectrometry. The result of the certification of samples from the contaminated soils with metals was very close to the calculated concentration except for the mercury samples, where it was possible that some of the mercury left the sample in the vaporization process (see Table 3).

Table 3
LIBS Mercury Samples (Prepared with Fisher sea sand and $HgCl_2$)

Name of Sample	Concentration Prepared in LIBS Lab, ppm	Concentration Certified by the Analytical Lab, ppm
FHG0	0	0.302
FHG24	24	17.2
FHG110	110	38.6

Hardware Setup

The WES LIBS instrumentation and setup is compatible with the setup at UNL. UNL has been under contract with WES to provide start-up support as well as to assist in collecting preliminary data.

Basic setup

The LIBS experimental setup was mounted on an optical table (1.2 by 2.4 m). The setup consists of an excitation laser, focusing optics, spectrometer, control electronics, and data acquisition hardware. The excitation laser is an Nd:YAG laser Continuum Surelite operating at a wavelength of 1.064 μm. It is capable of producing a 300-mJ, 7-ns pulse at a 20-Hz repetition rate. The output beam is approximately 6 mm in diameter. The

Nd:YAG laser was selected due to its relative high pulse energy, short pulse duration, ease of maintenance, safety (does not require or generate toxic gases), small size, and cost-effectiveness. A 5-mW red HeNe laser was coaligned and used to aid in aligning the Nd:YAG beam. The HeNe laser was placed next to the Nd:YAG and reflects off a mirror before being coaligned on a high-energy beam sampler. The beam splitter performs the dual function of coaligning the two beams and sampling the Nd:YAG beam for pulse energy measurements. Most (96 percent) of the Nd:YAG beam transits the beam splitter and passes through a bi-concave lens of 25.4 mm in diameter and focal length of -50 mm, and is expanded and passes through a plano-convex lens 50 mm in diameter and focal length of +127 mm, where the beam is collimated at a diameter of approximated 15 mm. See Figure 1 for the experimental LIBS equipment layout used for all liquid sample tests.

Liquid sample setup

The collimated beam then is incident on the entrance lens/window of the sample cell (see Figure 1). The sample cell is a polyvinyl chloride block machined to provide a central fluid reservoir and an entrance and exit window port. The breakdown occurs within the bulk liquid approximately 1.5 cm into the liquid. The light is then collected by a lens and imaged on the entrance slit of the spectrometer.

Soil sample setup

The same basic setup was used for the soil experiments except that the collimated beam was reflected down by a mirror at a 45-deg angle to allow excitation on the surface of the sample and passes through a plano convex lens of 30-mm diam and focal length of +50 mm, where the beam is focused over the sample as shown in Figure 2. The sample is mounted on a rotation table where it is turned so that a fresh sample surface is exposed for each excitation. The diameter of the sample holder is 100 mm. The diameter of the focused beam on the sample is approximately 1 mm, and it delivers approximately 100 mJ of energy per pulse. This produces power density on the order of 5 to 10 GW/cm^2. The light emitted by the plasma is collected through a 1-m optic cable, consisting of a bundle of 25 optical fibers, and is transmitted to lens and to slit at the entrance of the spectrometer.

Instrumentation

The spectrometer consists of an Instruments S.A. model HR 640, which has a focal length of 0.64 m and is equipped with a grating (early measurements = 600 grooves/mm; later measurements = 2,400 grooves/mm) controlled by computer, and a Princeton Instruments micro channel plate intensified 1024-element red-blue optimized silicon photodiode array. The

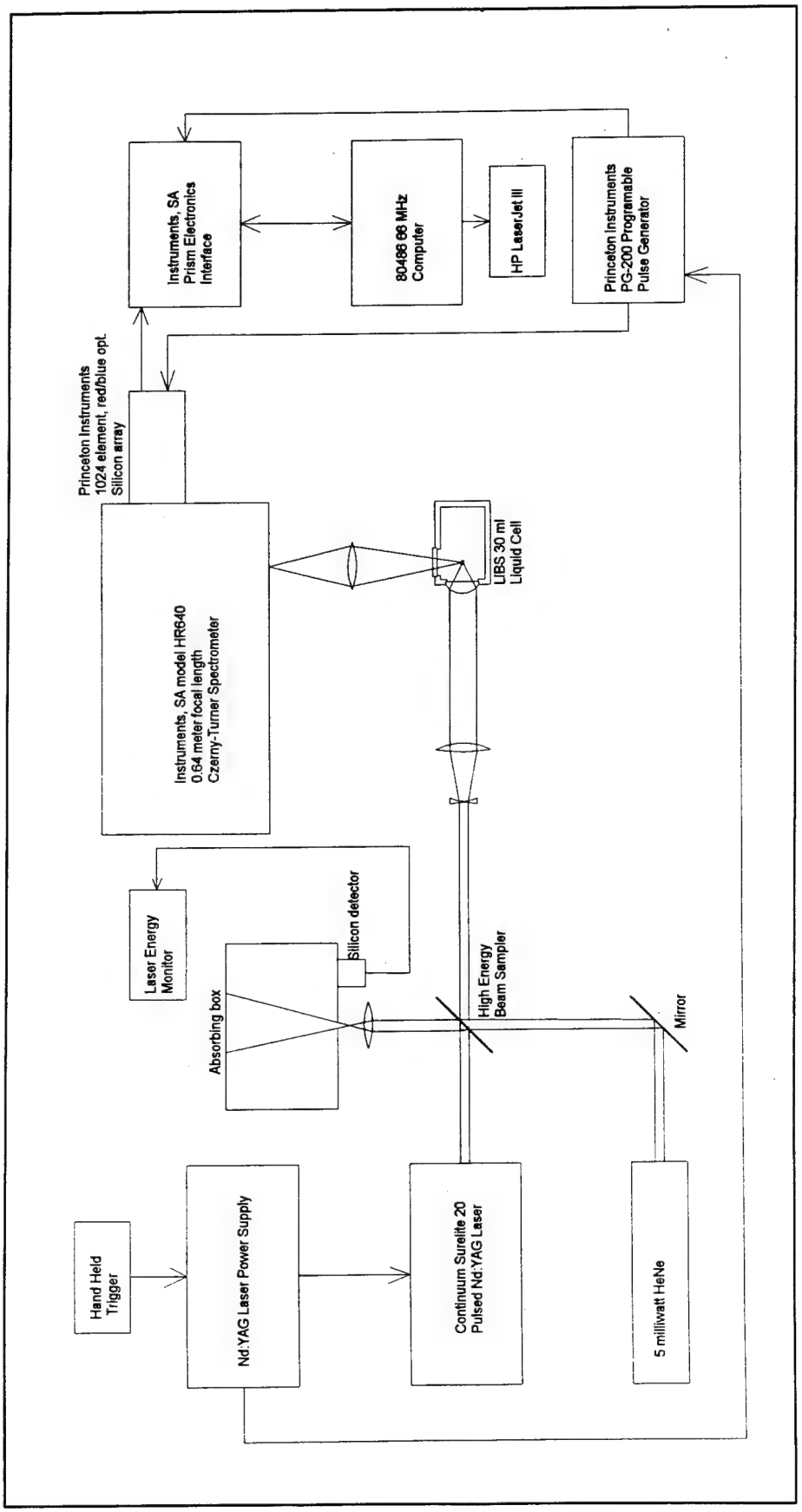

Figure 1. LIBS setup—liquid sample

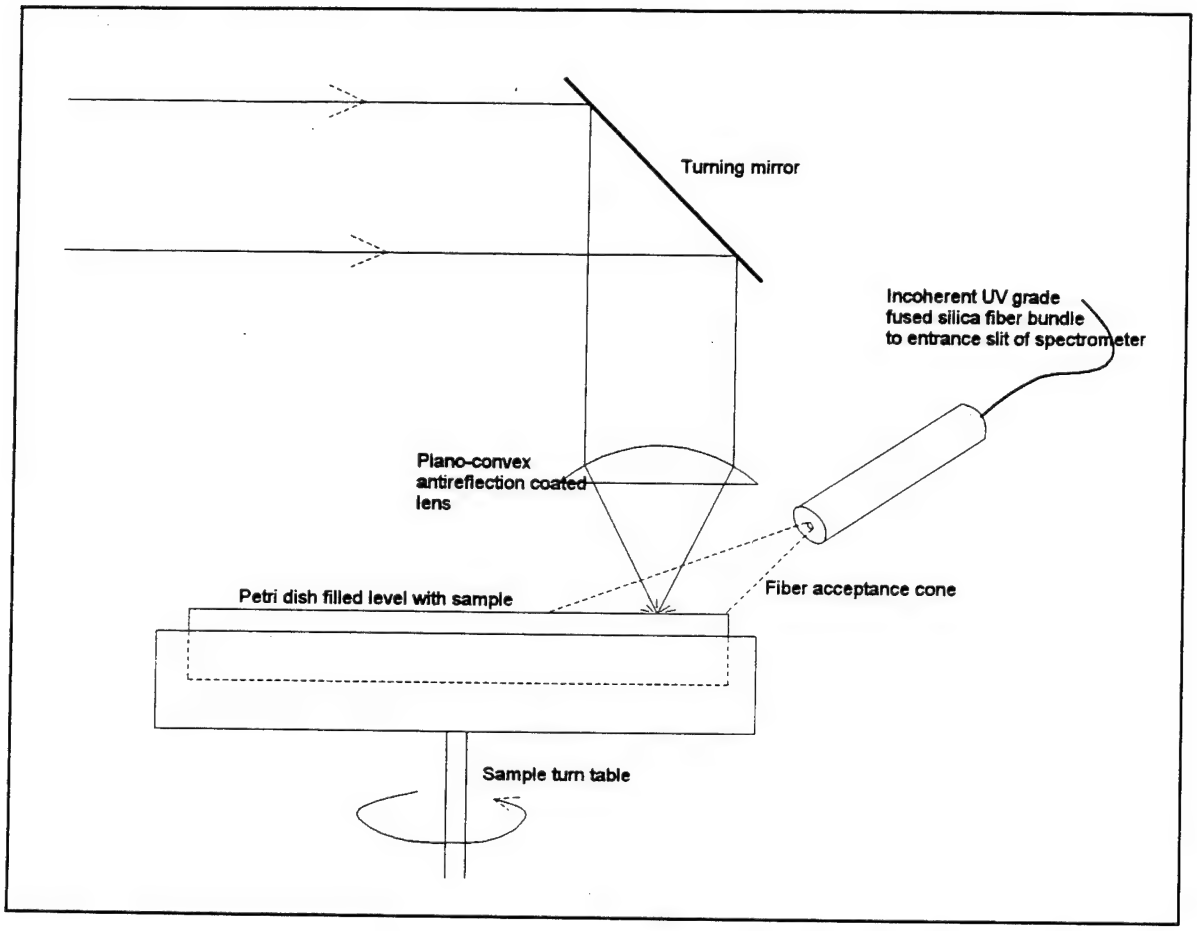

Figure 2. LIBS setup—soil sample

detector is controlled by a Princeton Instruments PG 200 programmable pulse generator. The detector is coupled to an Instruments SA Prism electronics interface data acquisition unit that is interfaced to a 486DX2 66 MHz computer that runs the Prism data acquisition software.

3 Experimental Considerations

Data Collection Controls

A LIBS spectral trace used for analysis and evaluation consists of 36 averaged experimental spectra. The Prism software package can automatically acquire and average 1 to 99 separate acquisitions into a single spectral plot. This averaging is done to reduce error due to inhomogeneity in the sample matrix and shot-to-shot variations. The process of collecting a data set begins with a hand-triggered control that triggers the laser. At the same time that the laser is fired, the laser controller activates the pulse generator of the instrumentation, which has selective delay (termed "gate delay"), before sending a high-voltage trigger pulse of a length equal to the desired integration time (termed "gate width") to the detector. The detector integrates only during the presence of the high-voltage pulse. The data are then stored in the Prism acquisition buffer. Ten microseconds later, the data are transferred to a temporary file in the computer. This process is repeated until the completion of the data set (36 times). At the end of the data set, the computer restores all the temporary files and converts them to permanent data files for further analysis.

The LIBS electronics instrumentation configuration was customized to improve the speed of the data collection. In addition, several macros were written to speed up the analysis of the data.

Resolution Issues

Instrumentation problems with the data acquisition from the soil samples were encountered in late FY93. The resolution obtained by combination of a 0.64-m spectrometer and a grating with a groove density of 600 grooves/mm (the pixel spectral resolution was 0.032 nm) for the soils samples was insufficient to separate the contaminant peaks from the soil background peaks (see Figures 3-6). Due to the complex chemical composition of the soil samples, a correspondingly complex background containing multiple peaks from the soil is unavoidable. This increases the difficulty of extracting the contaminant peaks. The previous experiments with water solutions did not have this

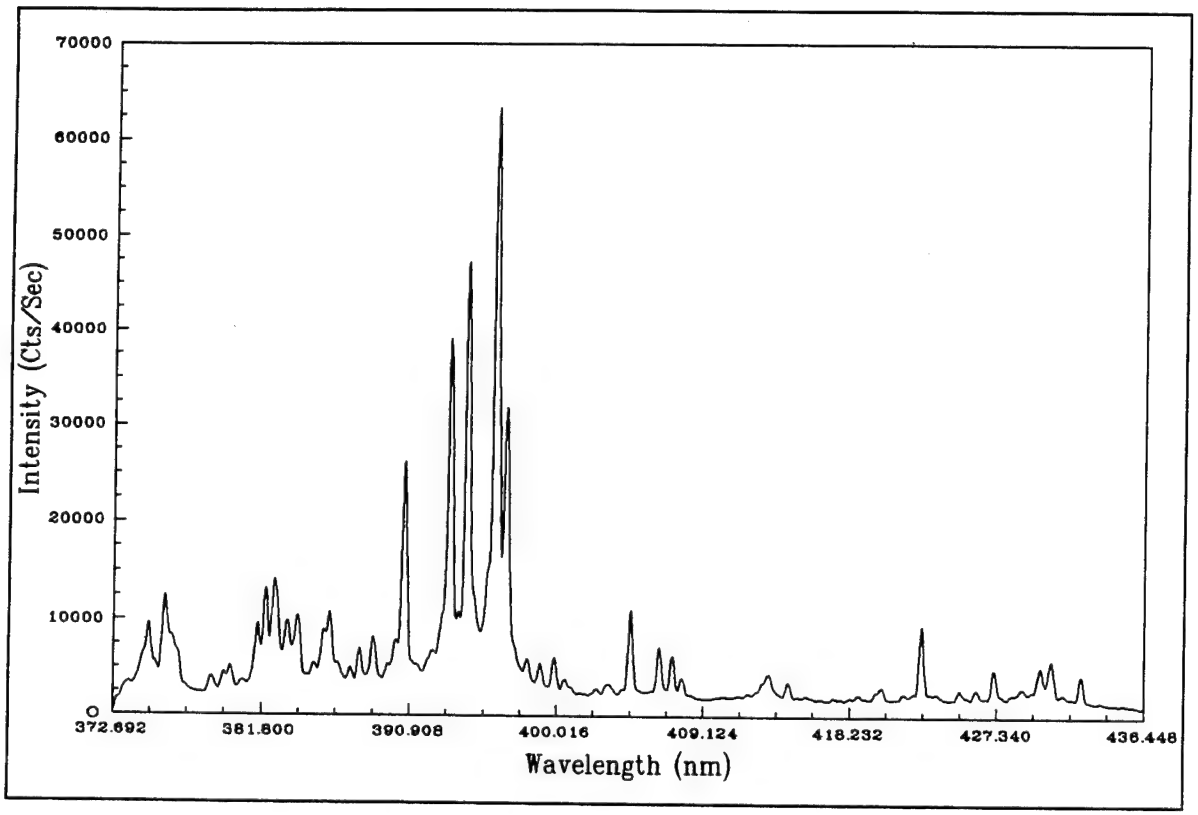

Figure 3. Spectrum of Fisher sea sand using a 600-groove/mm grating

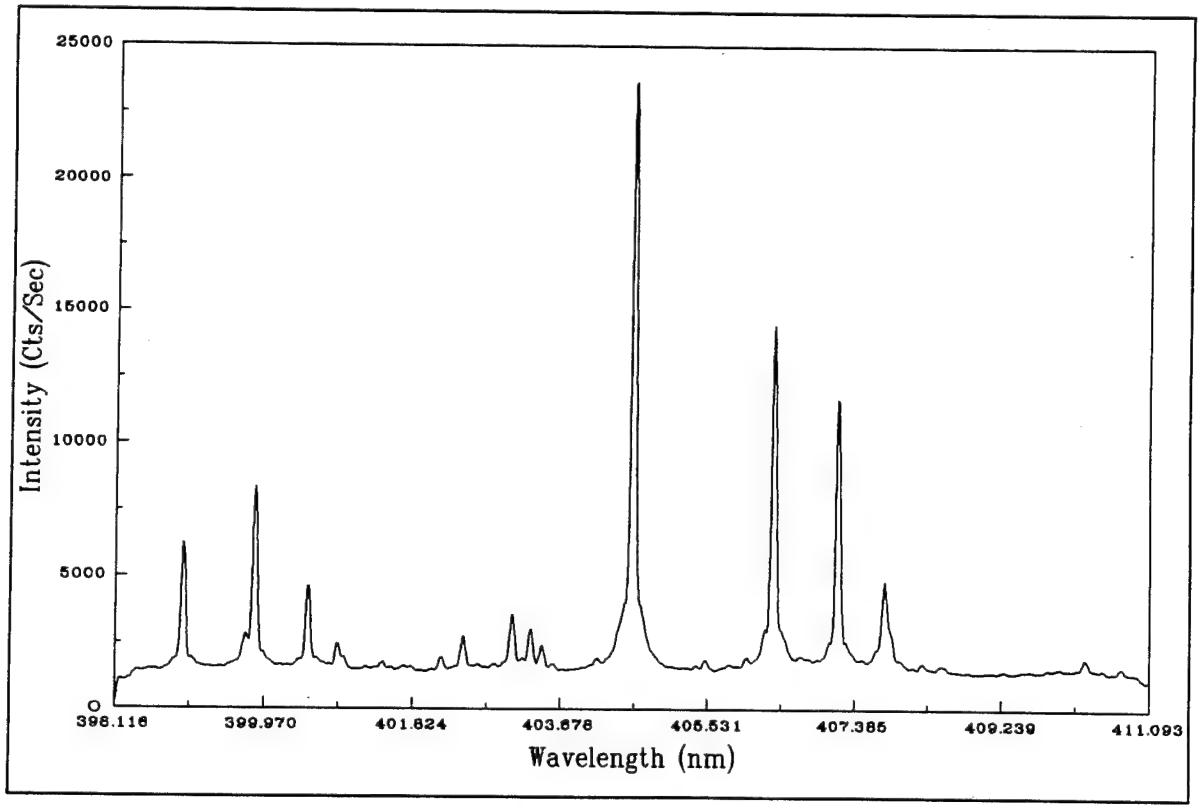

Figure 4. Spectrum of Fisher sea sand using a 2,400-groove/mm grating

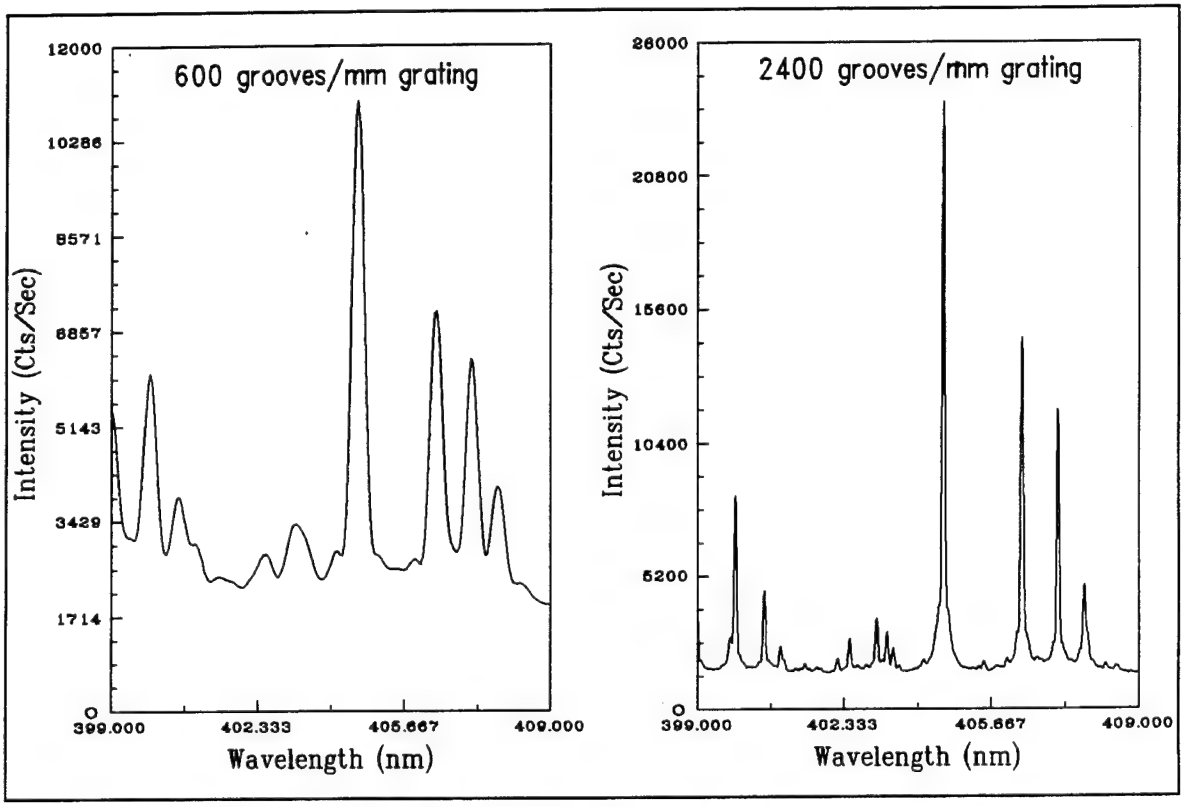

Figure 5. Comparison of resolution between the 600- and 2,400-groove/mm grating

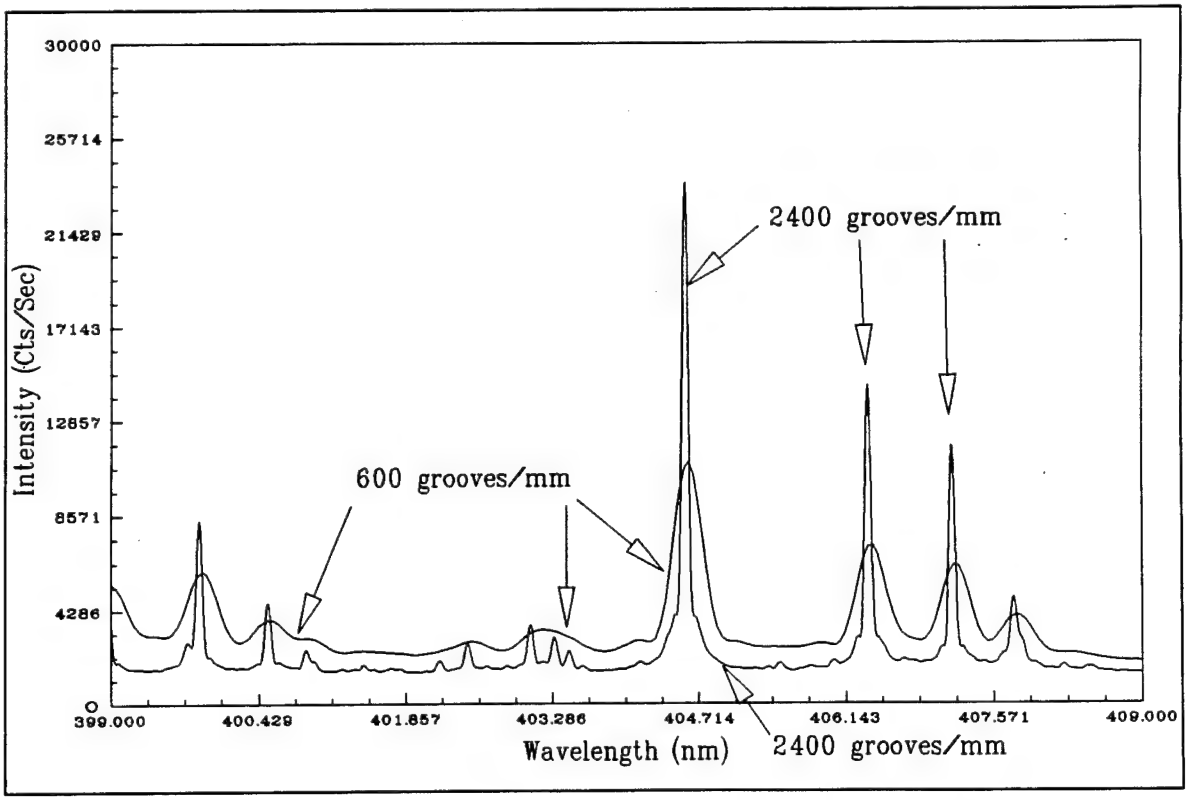

Figure 6. Overlap comparison of spectra using 600- and 2,400-groove/mm grating

problem of a large background of multiple peaks, so the discrimination of contaminant peaks could be accomplished with the low resolution grating.

Due to this problem, the spectrometer was equipped with a new 2,400-groove/mm grating to improve spectral resolution. The improved spectral resolution of the LIBS spectrometer is 0.008 nm (see Figures 4-6), and each spectrum collected covers a range of 13 nm.

Energy Level Issues

Adjustments and alignment of the optical paths were made to improve the optical throughput. These adjustments helped improve the plasma generation as well as the detection of the emission spectra. The fiber optic bundle used to collect the plasma emission was relocated to a position close to the breakdown area at approximately 2.5 cm and at an angle of approximately 20 deg to the surface normal. On the entrance of the spectrometer, the fiber was realigned and the lenses adjusted to maximize the signal in the spectrometer; the slit opening was adjusted to an approximated 10 μm. The lenses on the laser transmit path were realigned to an optimum position for minimum energy losses and a better focus over the soil sample, generating a stronger breakdown.

The factors that have major impact on LIBS data are the moisture content of the soil sample, the data collection parameters, and the laser energy. A soil sample that contains a high-moisture content will produce a lower intensity plasma emission. This is due to the large fraction of the laser energy consumed in vaporization of the water present in the soil sample. As a consequence, the result is fewer photons being emitted though the recombination process along with lower signal to noise ratios and a significant reduction in the amount of information about the contaminants present in the soil samples.

The plasma intensity is proportional to the amount of laser energy incident on a sample. If too much energy is applied, the resulting flash from the plasma will saturate the detector, obscuring smaller peaks. A low-energy laser pulse can fail to fully ionize the sample, thereby failing to excite the peaks of interest if the sample contains a low concentration of the contaminant. Breakdown can be created on a dry soil by using only 30 mJ of laser energy (see Figures 7 and 8). For best results, it is thus necessary to determine a laser energy that is a trade-off between these two extremes. The current experimental setup uses pulses of laser energy of about 100 mJ.

Detector and Data Processing Issues

The signal strength basically depends on three important factors: the intensity of plasma, the length of gate delay, and the gate width of the detector. The gate delay is the amount of time delay after the laser is fired before data

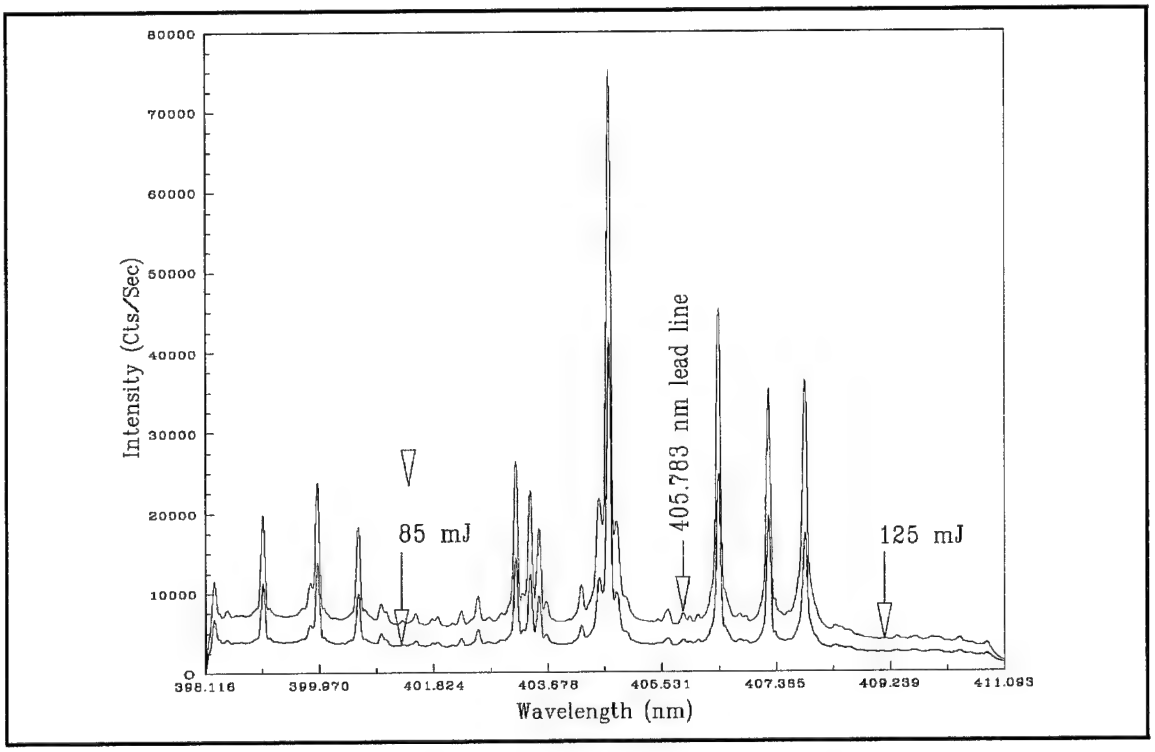

Figure 7. Spectra of Yuma sand at laser energies of 125 and 85 mJ with 7.71 ppm of Pb

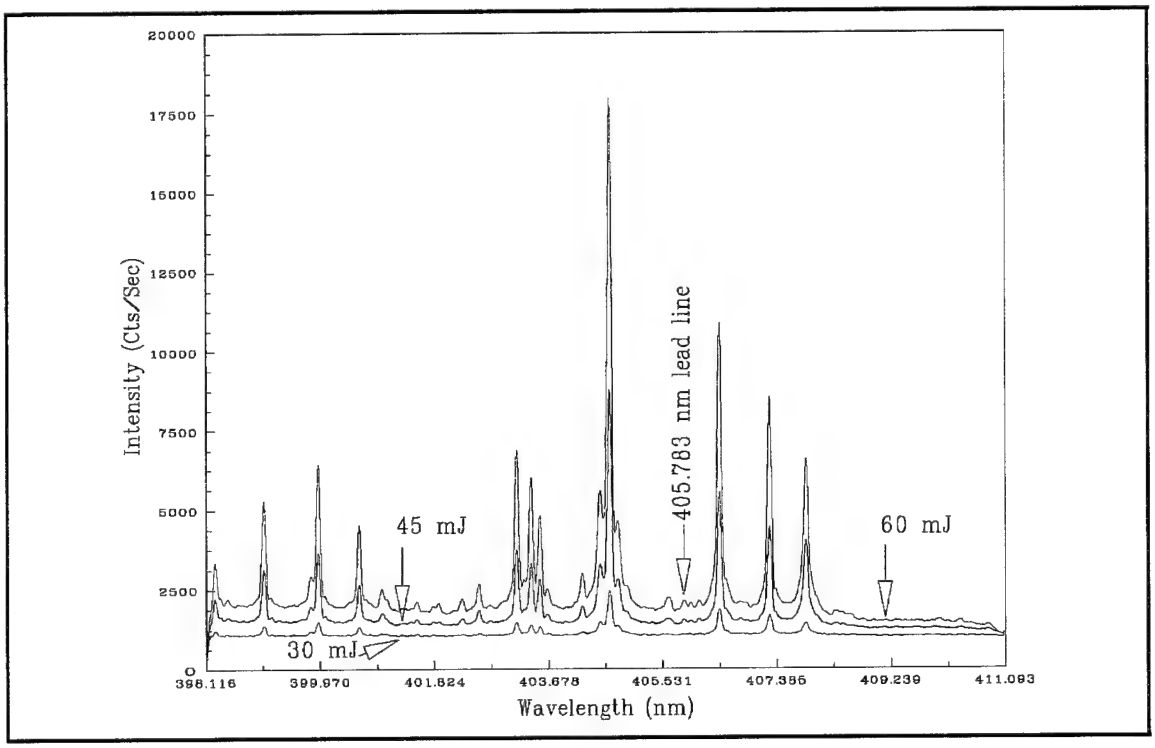

Figure 8. Spectra of Yuma sand at laser energies of 60, 45, and 30 mJ with 7.71 ppm

collection is begun. This time usually is short and varies from nanoseconds to 1 μs.

The gate width is the amount of time used for data collection and usually varies from 5 ns to milliseconds. The gate delay is the most difficult parameter to select. It has been experimentally observed that the optimum gate delay is a function of plasma intensity as well as the lifetime of the excited state of the contaminant. If data collection begins too soon with respect to the principal emission, then the spectra obtained will contain signals from the broad band emission of the plasma in addition to the spectra of interest. This will be apparent from a general elevation in the background intensity recorded by the detector as show in Figure 9. If data collection begins too late with respect to the principal emission, it is possible to lose important information of interest (see Figure 10).

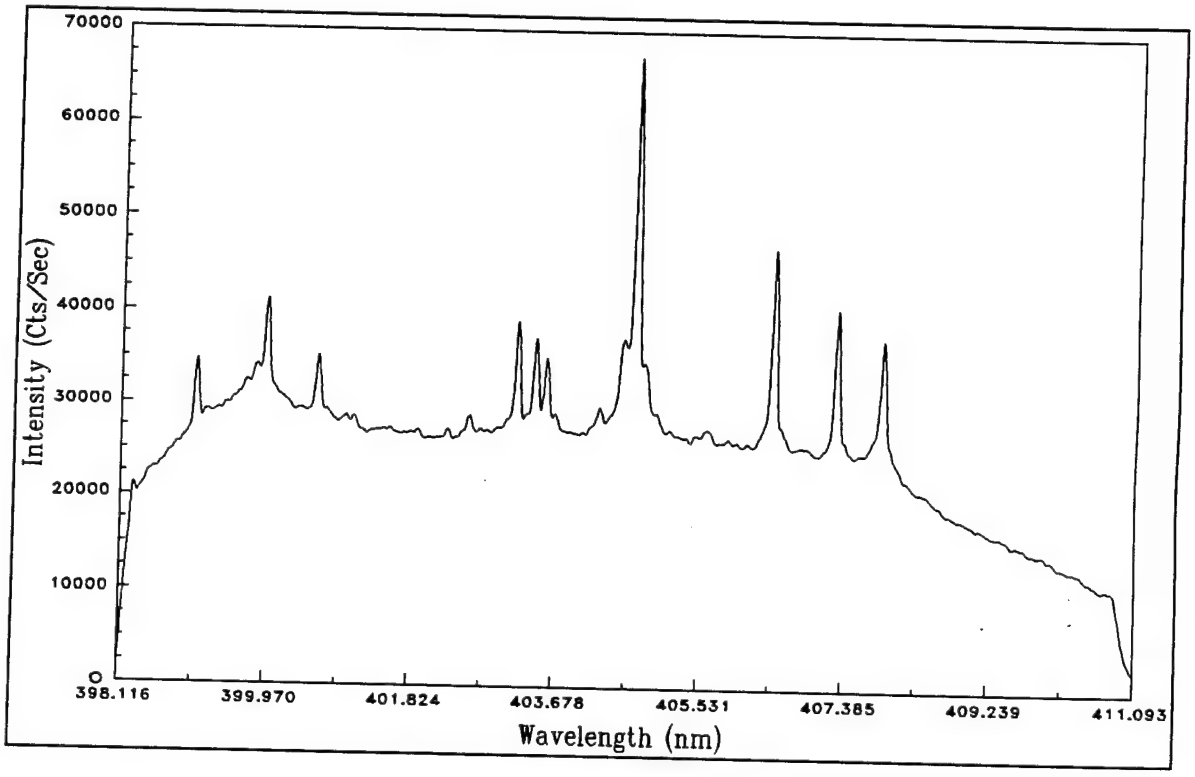

Figure 9. Collection of broad band emission and Yuma sand spectrum at gate delay of 64 ns and gate width of 100 μs

Optimization of the gate delay parameters was done by collecting measurements from a lead plasma using a gate delay that ranged from 75 to 1,200 ns in steps of 25 ns and a gate width of 10 ns with 100 mJ of laser energy and a slit opening of 10 μm. The sample in the series of measurements was a disk of pure solid lead (see Figures 11-13). The lead line used was at 405.783 nm, and the peak intensity of this line was plotted against the time delay (see Figure 14).

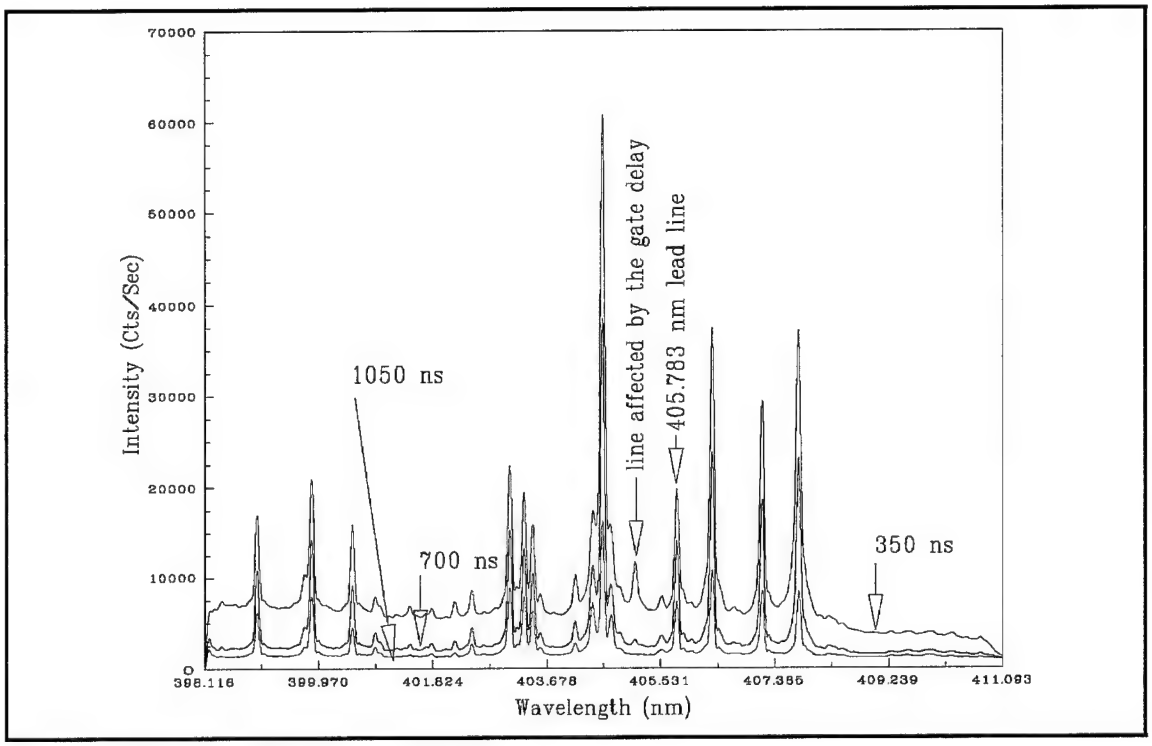

Figure 10. Spectra of Yuma sand containing 132 ppm of lead at different gate delays and 100-μs gate width (Note emission line affected by gate delay)

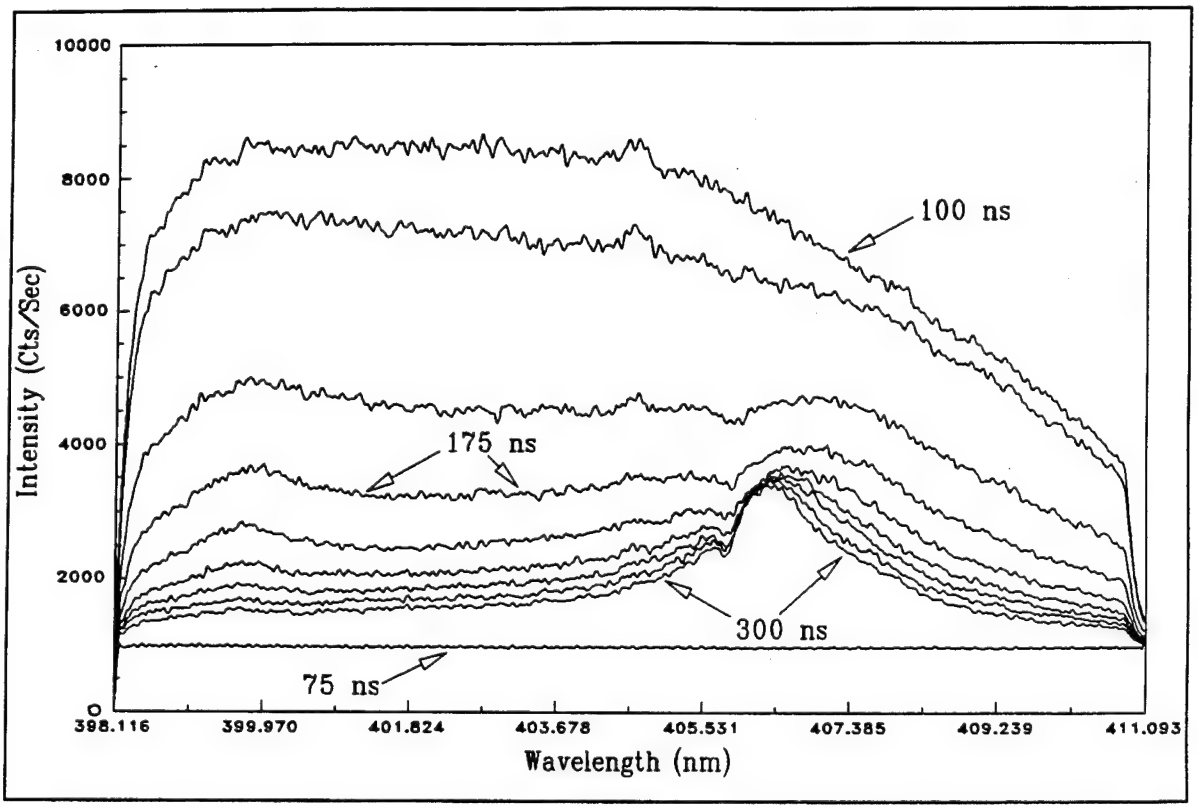

Figure 11. Spectra of behavior of lead plasma from beginning of broad band emission until 300 ns (Increments of gate delay shown are 25 ns at 10-ns gate width. At 75 ns, no emission occurs. At 100 ns, broad band emission is decaying rapidly, and at 150 ns, spectrum is beginning to show shape of lead peak)

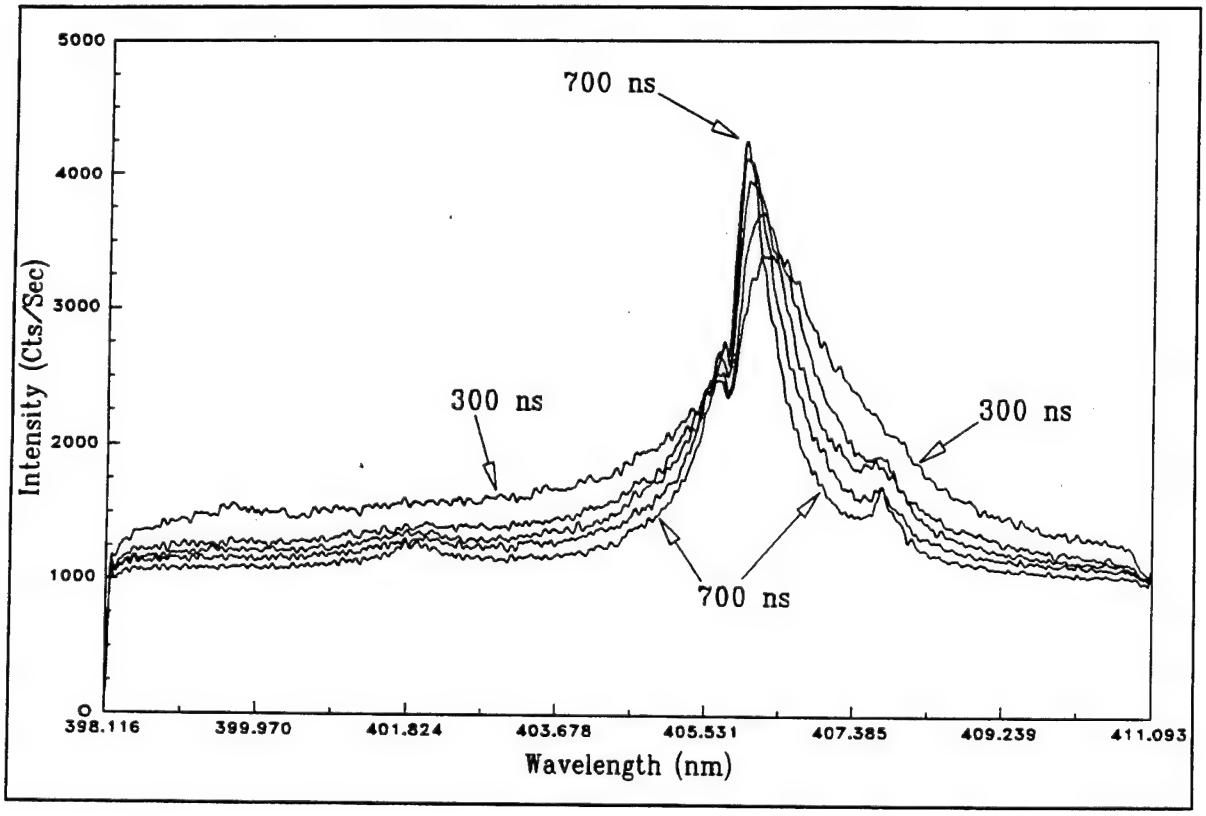

Figure 12. Plasma time evolution behavior from 300 to 700 ns (Increments of gate delay are 100 ns at 10-ns gate width. After 300 ns, lead peak continues to grow until 750 ns and broad band continues to decay)

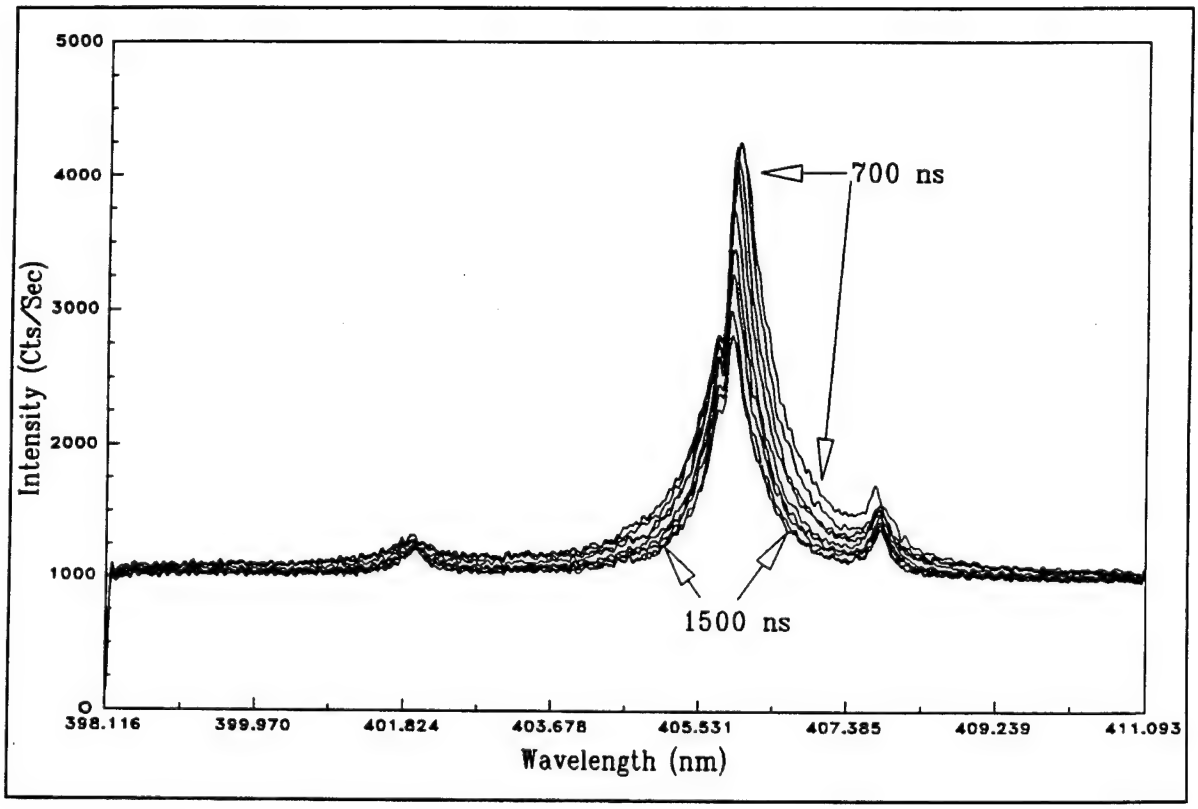

Figure 13. Plasma time evolution behavior from 700 to 1,500 ns (Increments of gate delay shown are 100 ns at 10-ns gate width. After 750 ns, lead plasma decays slowly out to about 40 μs)

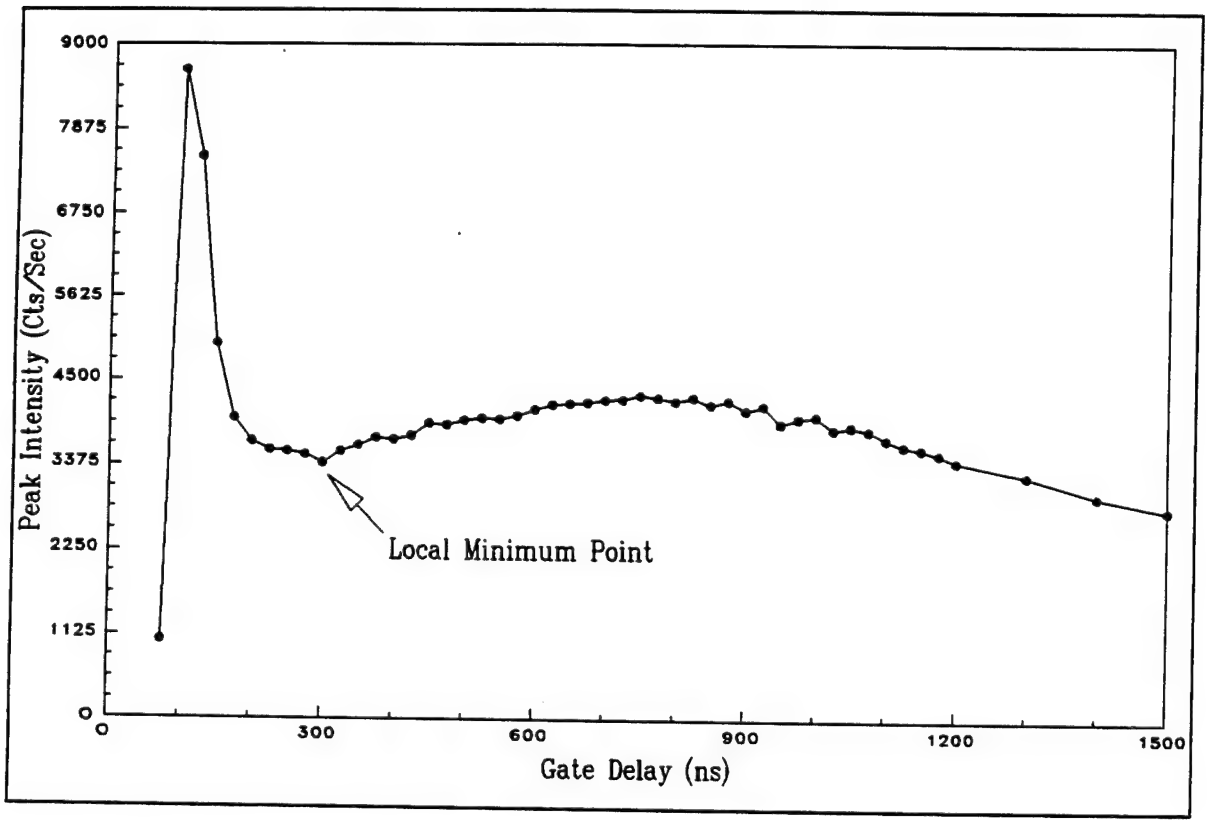

Figure 14. Plot of lead plasma behavior at 100 mJ of laser energy

4 LIBS Data Collection

Experiments were performed in FY 93 for determining the detection of heavy metals in water and soil samples using LIBS and some detection limits calculations. As indicated above, LIBS experimental techniques and parameters are evolving issues. Because these parameters have a major impact on interpretation of results, the presentation of spectral data will be divided into two parts, each being characterized by its own set of data collection parameters.

Early Experiments

Data collection parameters for early LIBS testing at WES included the use of a 600-groove/mm grating, a gate delay of 300 ns, a gate width of 5 μs, a slit opening of 10 μm, and laser energy of approximately 75 mJ.

Results of liquid sample experiments

Previous research data and preliminary experiments done at WES indicated that solid sample LIBS analysis was simpler than liquid sample testing. One reason was that early trials required removing the liquid samples cell from the optical table each time a different contaminant was used or each time the contaminant concentration was changed. Not only was the technique awkward and time-consuming, but also it was possible to add another variable to the interpretations process. The spark light from each test was imaged by a lens directly on the spectrometer entrance slit, and any movement of the liquid cell would move the spark image on the slit, potentially resulting in a strong variation in the received intensity. Thus, the following technique was developed to test a wide variety of concentrations in a single cell without moving the cell.

The goal of the liquid experiments was to test all samples without having to remove the sample cell from the optical table for each contaminant. A usable volume of low-concentration liquid was added to the cell for the first test. This liquid level was just above the top edge of the laser beam for the first sample. Small but progressively more concentrated additions were made to the liquid cell until the final concentration was reached. A program was

written in a spreadsheet format for calculating the exact amounts of liquid base solution needed to achieve certain concentrations. A starting volume of 25 ml was chosen for the cell whose total volume was 36.5 ml. Starting with a concentration of 22 ppb and gradually increasing volumes and increasing concentrations were added until the final concentration was about 1,500 ppm.

Initial tests were conducted with manganese solutions, and a strong resonant line was noted at 403 nm, which was then used to develop a calibration curve. The complete calibration curve for the manganese solutions is shown in Figure 15, and shows the increase in signal strength with increasing concentration. Each point represents an average of the 36 spectra collected.

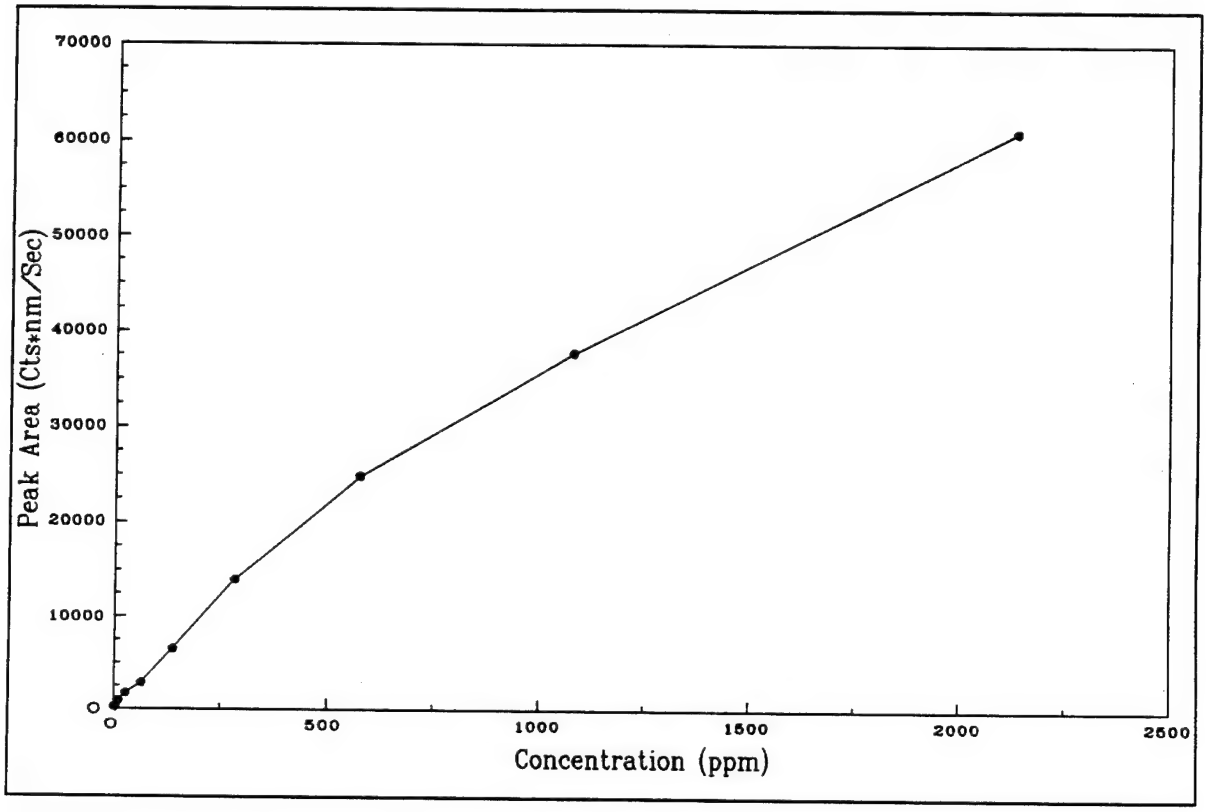

Figure 15. Calibration curve for Mn in water

The standard spectroscopic approach for evaluating the smallest concentration of an element in a solution or mixture that can be detected by the experimental technique intensities of the spectra being collected is the following equation:

$$C_L = \frac{Z^* S_B}{M}$$

where

C_L = detection limit

Z = constant (2, 3)

S_B = standard deviation of peak area calculation

M = slope of calibration curve

To determine a detection limit for the manganese solution, the slope of the calibration curve is determined near the lower concentration test points. The lower four data points of the calibration curve are shown in Figure 16. The standard deviation of the peak area was calculated from the individual 36 spectra collected. Using these plots, and employing a factor of $Z = 2$ times the standard deviation of the peak area calculation, the detection limit for manganese was calculated to be approximately 70 ppm. A plot of the spectral signatures (403-nm spectral line) of different concentrations of manganese is shown in Figure 17.

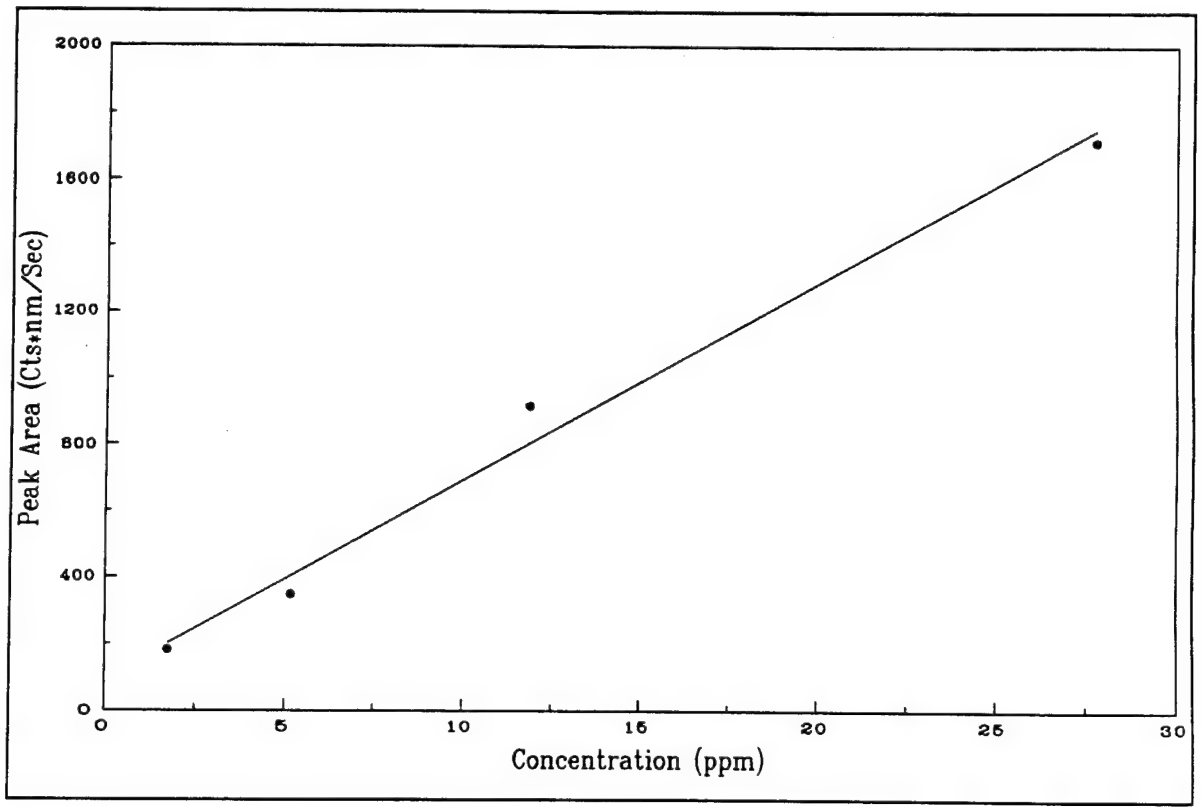

Figure 16. Lower portion of calibration curve for Mn in water

Tests of lead solutions revealed a strong spectral line at 405.78 nm, with a detection limit of approximately 300 ppm. Thallium tests produced a very strong peak at 337 nm, which was detectable at concentrations as low as 6 ppm. Chromium tests yielded a strong peak at 520.9 nm, which was

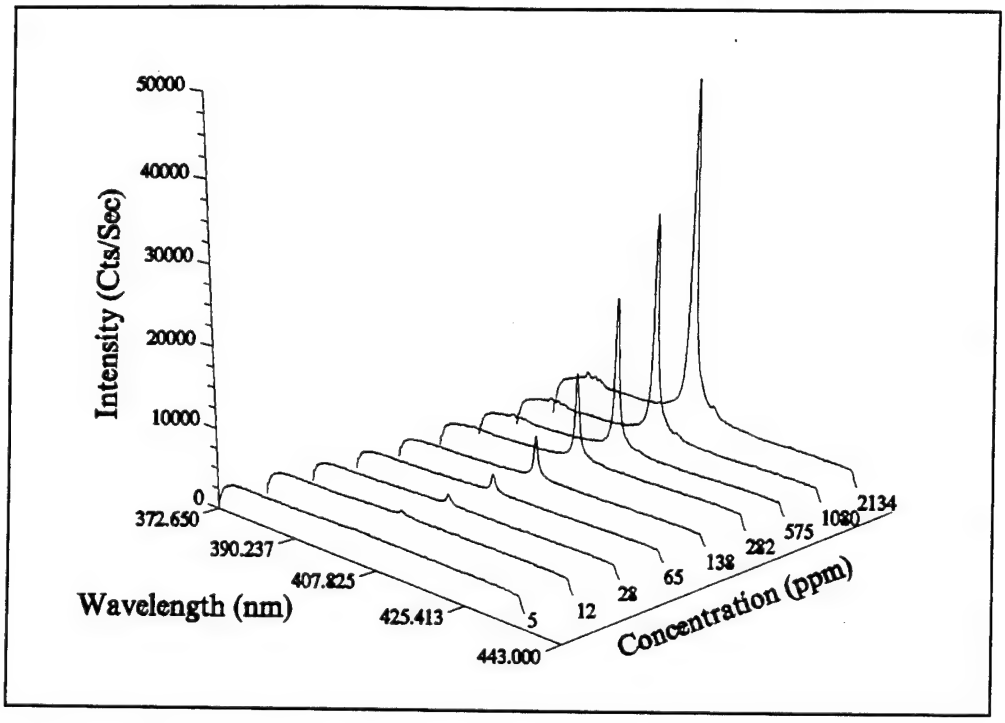

Figure 17. Spectral plots of Mn in water

detectable at concentrations of 100 to 150 ppm. Iron tests revealed one weak peak at 404.48 nm detectable only at the higher concentrations (1,500 ppm). Tests of copper solutions resulted in a broad emission region between 350 and 560 nm, but no definite peaks were detected. The tests performed at UNL with the excimer laser yielded spectral lines for aqueous samples of cobalt, iron, lead, manganese, chromium, and cadmium. Neither WES nor UNL tests were able to detect the other metals shown in Table 1 in solutions even at very high concentrations (10,000 ppm).

Results of pure metals experiments

A wealth of documented atomic spectra lines exists for the elements being studied here (Meggers, Corliss, and Scribner 1975; Robinson 1991). The spectral lines documented by spectroscopists over the last 50 years were created by various means including plasma arcs and flame emission studies. LIBS is a transient phenomenon with a limited amount of energy per pulse for sample vaporization and excitation. Early UNL experiments showed that testing the same samples with different operational wavelength lasers produced entirely different results. Note that if the line is excited, independent of method, it will have the same spectral location defined by the radiative transition. The purpose of the pure metal study was to determine which lines are likely to be produced via LIBS using a 1.064-μm Nd:YAG laser. The metals used for these experiments were lead, cadmium, chromium, and zinc. For the mercury test, HgCl was used. This compound is 85-percent mercury and safe and easier to work with than liquid mercury.

The pure metal experimental setup is virtually identical to the soil sample experimental setup. In all cases except for mercury, a small circular foil piece of metal was placed on the rotation table so that a new spot of metal was presented for each breakdown event. HgCl salt in a petri dish was used for mercury.

The results indicated that a tremendous number of lines were generated by the foil experiments. It should be noted that many of the lines seen are actually lines due to the breakdown of air as well as the metal of interest. Thus, there are many more lines in the spectral plots than one would expect from the metal alone (see Table 4, where the heavy metal spectra lines observed by using LIBS setup are from higher to lower emission intensity. The order of intensity could vary from setup to setup because of the different responses of the detectors used and the efficiency of the grating used).

Table 4
Spectral Lines Observed in Pure Metal Experiments

Lead nm	Chromium nm	Cadmium nm	Mercury[1] nm	Zinc nm
405.783	425.435	214.438	435.835	334.502
368.348	427.480	228.802	404.656	328.233
280.199	283.563	226.502	313.183	280.106
283.306	396.369	361.051	365.015	280.087
363.958	267.716	340.365	296.728	277.098
282.320	284.325	361.288	576.959	277.086
373.995	396.975	326.106	579.065	
287.332	425.435	231.284	253.652	
247.638	284.984	298.063	546.074	
357.274		288.077		
257.727		361.445		
401.964				
367.151				
416.803				

[1] HgCl was used instead of Hg.

Results of soil sample experiments

Due to the complex LIBS spectra of the soil samples, soils were first characterized without contamination present. After examination of uncontaminated soils, contaminated soils were analyzed by LIBS and compared. Contaminant peak detection was facilitated by comparison to the uncontaminated soils.

Calibration procedures similar to those used in the development of calibration curves for the liquid samples were used in the soil sample tests. To obtain an estimate of the detection limit, two concentrations of each element were tested, 100 and 500 ppm (Cespedes, Miles, and Lieberman 1993). Tests were done using all three soil matrices in their dry condition. The 500- and 100-ppm samples for each matrix were tested back to back without any spectrometer grating movement between the tests to reduce variations caused by laser power drift and spectrometer miscalibration. The background standard deviation was taken to be the standard deviation of the peak characteristic of interest at the lowest concentration of the calibration curve.

In order to establish the lowest detection limits, it was necessary to determine which irradiance measurement parameter best correlated with concentration while maintaining relatively low standard deviations. Raw peak intensities were investigated first, but variations in the strength of these peaks yielded high standard deviations and correspondingly high detection limits. Raw peak areas produced slightly better results but still had high standard deviations. The method chosen for the calibration of soil spectra was to ratio the metal peak area to an arbitrary small soil background peak within the same spectrum. Utilizing this ratio technique helped minimize the effects of spark intensity and sample volume variations, thereby lowering the calculated detection limits.

The strongest metal spectral peaks seen in the liquid sample and pure metal tests served as a guide for finding these relatively small spectral peaks amidst a much larger background. Direct superposition of the spectra at two different concentrations proved helpful in determining which contaminant peaks yielded the best detection limit. For example, a direct superposition of spectra is shown in Figure 18, where the 500-ppm lead sample spectrum is superimposed over the 100-ppm spectrum. Inspection of this plot shows the lead line of interest and the corresponding amplitude differences at 405.86 nm. Note that the amplitude values and shapes of the two spectra are very similar in the two files except in this region, thus highlighting the peak. Detection limits were calculated for any visible peaks corresponding to known contaminant lines. The weaker lines were analyzed in addition to the strong ones for completeness, but the best signal (i.e., the strongest line) should define the actual detection limit.

The results of the dry soil tests are summarized in Table 5. Cadmium tests in sand provided three peaks that could be used for detection-limit calculations. A soil reference peak of 212.34 nm was chosen for normalization. The pure soil sample spectra were examined to verify that this peak was not caused by the contaminant or the contaminant carrier acid. The detection limits were 142, 149, and 300 ppm, respectively, for the 226-, 228-, and 214-nm cadmium line. Clearly, the first or second peak is better for quantitative purposes and should represent the measured detection limit. In general, the detection limits in sand were lower than in the other two soil types. This effect is believed to be due to the comparatively larger size of the sand particles. Detection limits were also lower for the dryer samples. This was due to

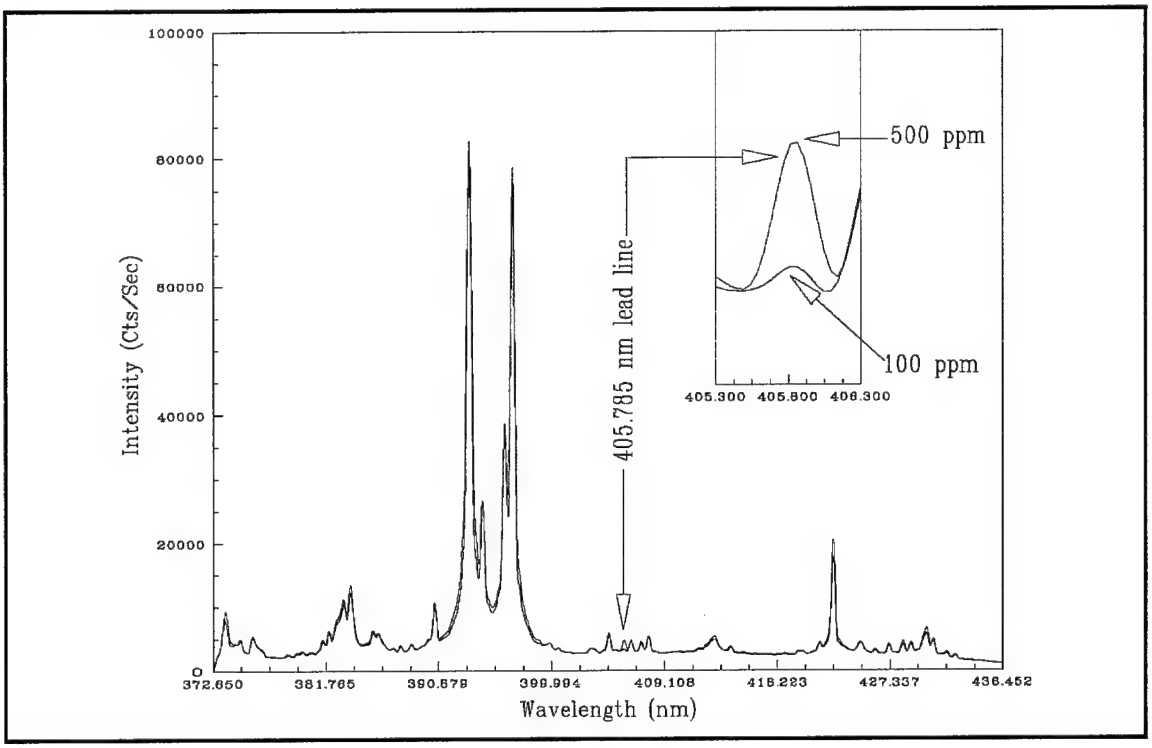

Figure 18. Superimposed spectra of lead in Yuma sand at approximated 100 and 500 ppm

the fact that water in the sample has a high heat capacity, and a portion of the laser energy is used in vaporizing the water. The reduced energy available to ionize the soil results in a weaker spark and correspondingly weakened spectral signatures.

The detection limit of chromium in sand was approximately 230 ppm using the 425.5- and 359-nm peaks. Only one peak was detected in the lead tests (405.83 nm), which resulted in a detection limit of 106 ppm for the dry sand matrix. Zinc was found in sand at a limit of approximately 219 ppm. Only one line was evident in the clay tests of zinc, and it resulted in a detection limit of 712 ppm. Several zinc lines were evident in silt, with the most sensitive being at 213.89 nm with a detection limit of 489 ppm.

Previous tests on liquid samples performed by UNL and WES had failed to excite or identify any mercury lines either with the excimer or the Nd:YAG. As Table 5 indicates, soil samples with mercury concentrations as high as 2,400 ppm also failed to reveal any peaks. An additional test was performed on a sample of pure crystalline mercury chloride. In this case, mercury peaks were detected, with the strongest lines occurring at 253.65, 296.68, 312.56, 313.15, 364.96, 404.65, 435.84, 576.95, and 579.06 nm. Unfortunately, extremely high concentrations of mercury (850,000 ppm) were required to generate these lines. The lack of detectable lines in both the liquid and soil tests indicates that there were problems with the LIBS technique for the detection of mercury.

Table 5
Results of Dry Soil Sample Test

Heavy Metal	Soil	Test No.	Heavy Metal Line Used, nm	Background Line Used nm	Detection Limit ppm
Lead	Yuma sand	1	405.783	404.62	106
	Clay	1	405.783	404.62	1,022
	Silt	1	405.783	404.62	632
Chromium	Yuma sand	1	425.435	422.74	233
		2	360.533	334.93	260
		3	359.349	334.93	219
		4	206.149	212.43	1,592
	Clay	1	359.304	344.30	324
		2	284.325	285.24	436
	Silt	1	359.349	344.32	458
Cadmium	Yuma sand	1	226.502	212.34	142
		2	228.802	212.34	149
		3	214.438	212.34	300
	Clay	1	226.502	212.34	633
	Silt	1	214.438	212.34	741
Mercury	Yuma sand	1			N/A
	Clay	1			N/A
	Silt	1			N/A
Zinc	Yuma sand	1	206.200	221.20	252
		2	202.548	221.20	219
	Clay	1	202.548	212.45	712
	Silt	1	213.856	212.45	503
		2	202.548	212.45	489
		3	206.200	212.45	2,613

Later Measurements

One possibility for the lack of detectable Hg lines in the early experiments was that the mercury emission occurred before or after the data collection; the previous measurement parameters of a gate delay of 300 ns and a gate width of 5 μs were questioned. Samples of HgCl (85-percent Hg) were used in measurements made with the early LIBS setup using gate delays that ranged from 100 to 900 ns in increments of 100 ns and a gate width of 10 ns; in addition, parameter values of a 3,500-μm slit opening and a 125-mJ laser energy were selected. (See Figures 19 and 20 for the spectra that were collected with these parameters.)

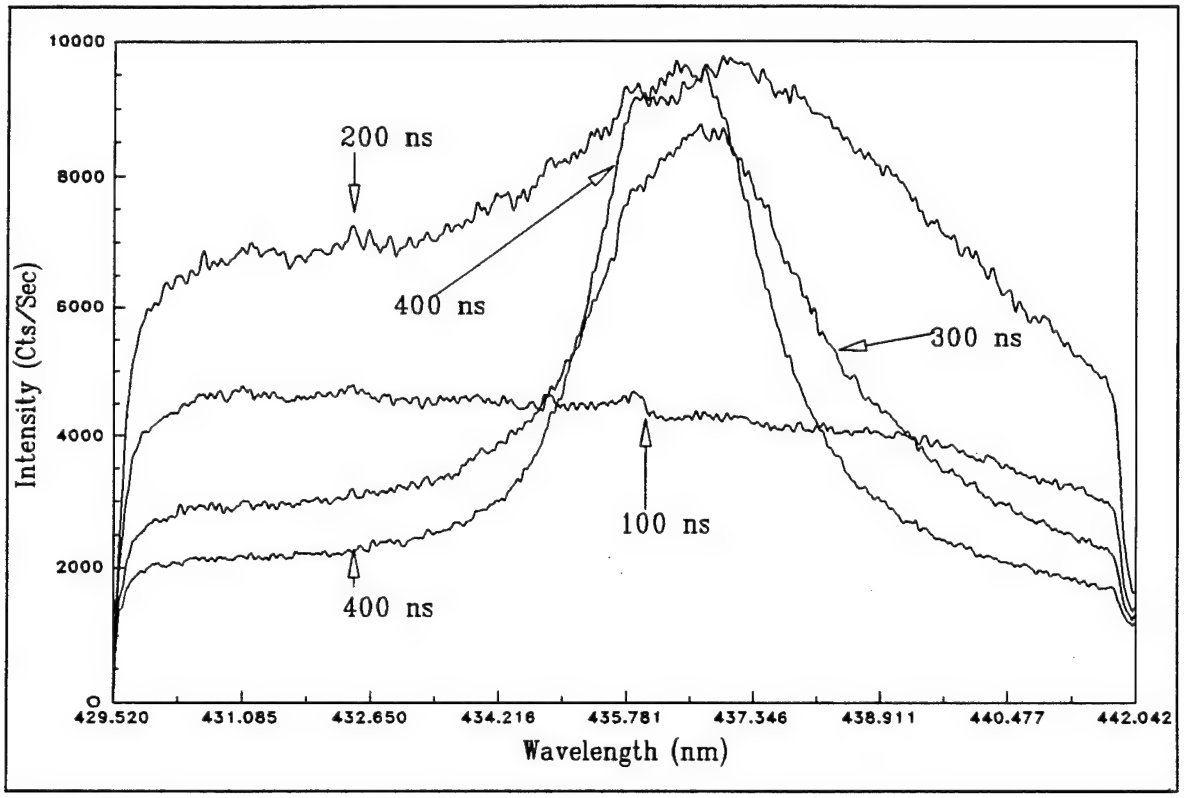

Figure 19. Spectra of mercury from HgCl at different gate delays

The data were reduced, and the intensity of the 435.835-nm peak of Hg was plotted against the gate delay. Results obtained from this experiment indicate that the emission begins around 300 ns with the strongest emission between 350 and 550 ns (see Figure 21).

Detection of mercury was a challenge. There were possible systematic errors in the production of the mercury samples that were used in measurements. It was found that the mercury compounds used were reduced in the soil sample by the presence of heat. The procedure for generating these samples was to mix the heavy metal solution with the soil and then dry the mixture for at least 24 hr at an oven temperature of 100 °C. It was later

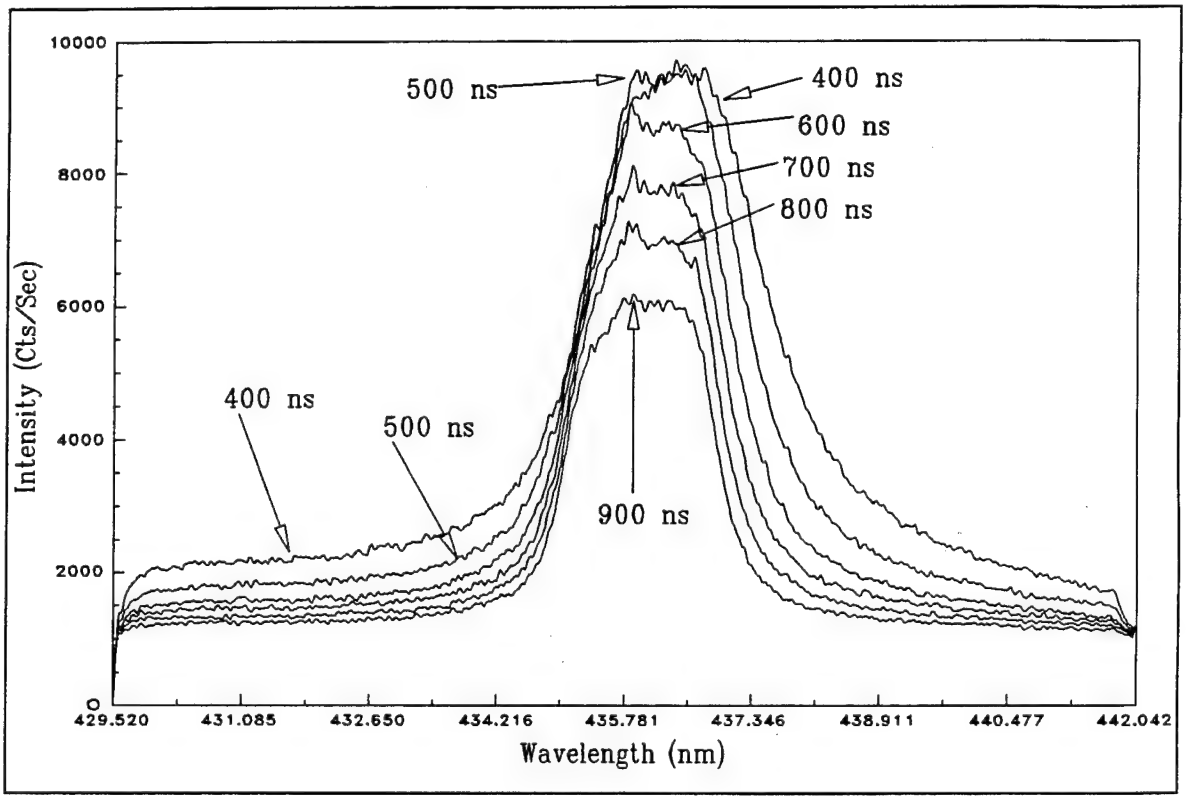

Figure 20. Mercury spectra from HgCl at different gate delays

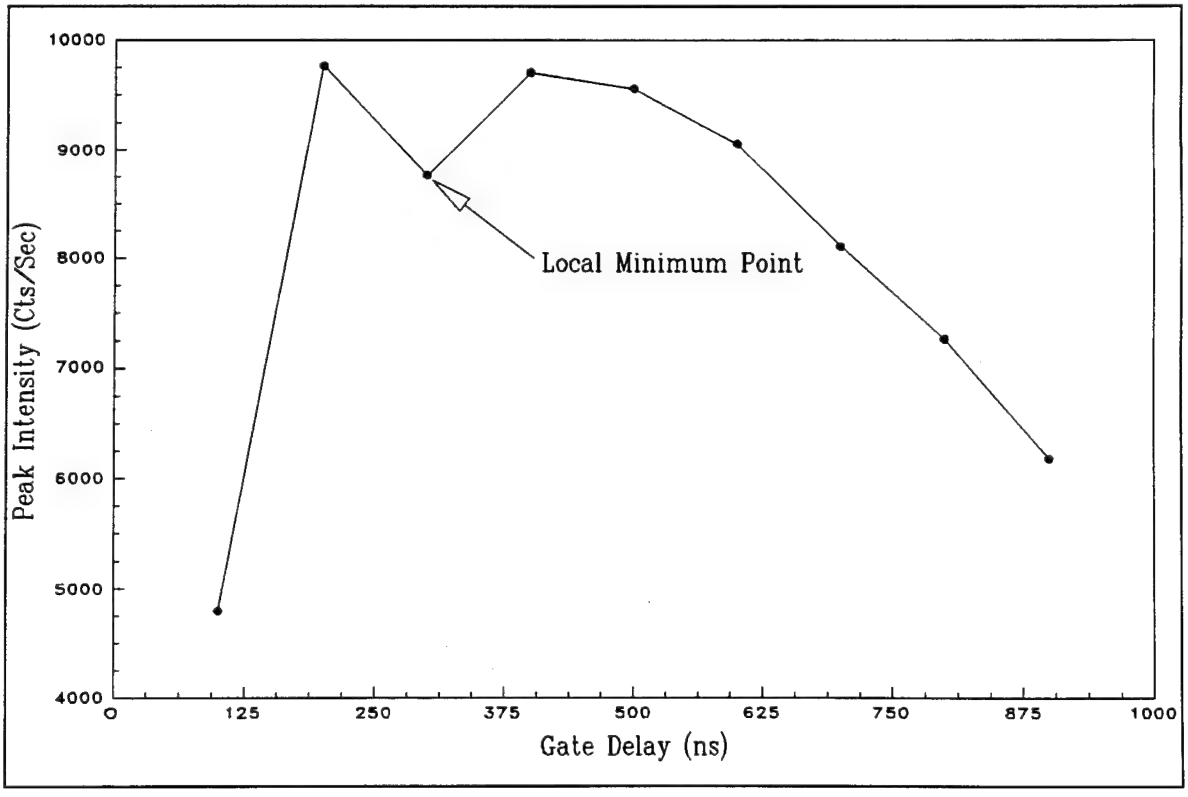

Figure 21. Behavior of 435.835-nm line of mercury in HgCl

discovered that this step of the process was producing mercury vapor during heating, resulting in a much lower contaminant concentration in the sample. Subsequent experiments used the new sample preparation procedure that involved the use of acetone, which was discussed in the sample preparation section.

The data collection parameter for these later measurements also took advantage of the improved detector grating of 2,400 grooves/mm and included a gate delay of 350 ns, a gate width of 100 μs, a slit opening of 10 μm, and laser energy of approximate 100 mJ.

The results for mercury obtained from the acetone technique were satisfactory. For an example, see Figure 22, which contains a composite of two different spectra at very low mercury concentrations and the background concentration. Note that the number of samples was not sufficient for the proper detection of analysis of detection limit, but it was expected that LIBS will detect Hg below 10 ppm without significant problems. Research into detection limits of mercury will continue when the LIBS prototype sensor is built.

Additional problems with the detection of mercury were encountered when the peak of the principal lines of Hg on the spectra were overlapped by peaks in the background. See Figures 23-28, where the mercury concentration was approximately 7,800 ppm in Yuma sand. Data found in these figures were collected at approximately 75 mJ of laser energy. As a result of these experimental results, it was decided that extraction of peaks for the identification of mercury at low concentrations would be limited to the 435.835-nm line.

All the LIBS research reported above was done under laboratory conditions, where LIBS has demonstrated to be a powerful tool in the in the detection of heavy metals. The question remains, however, of how the LIBS measurement and data analysis technique will fare against real test site soils? The following Figures 29-31 contain LIBS spectra of soils from Department of Defense (DoD) sites contaminated with heavy metals, and, while still not representing field tests of the technology, do indicate the strong potential for LIBS as a field heavy metal contaminant-detection instrument.

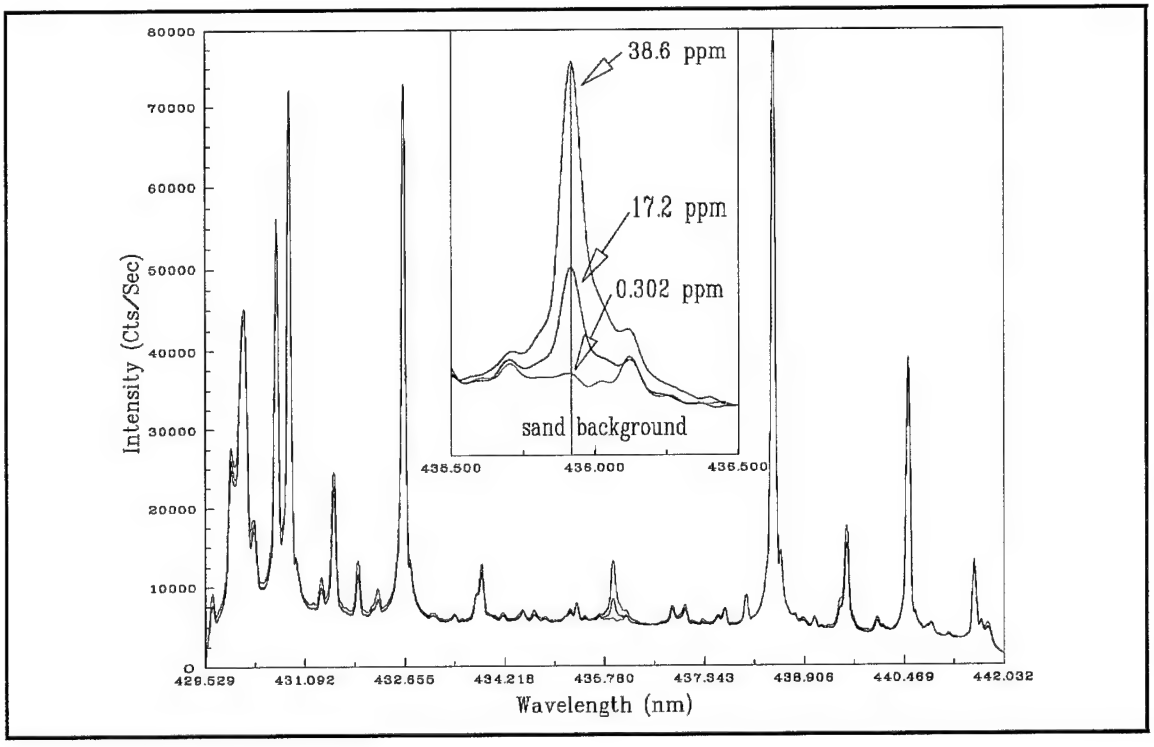

Figure 22. Spectra of 435.835-nm line of mercury in Fisher sea sand at different Hg concentrations

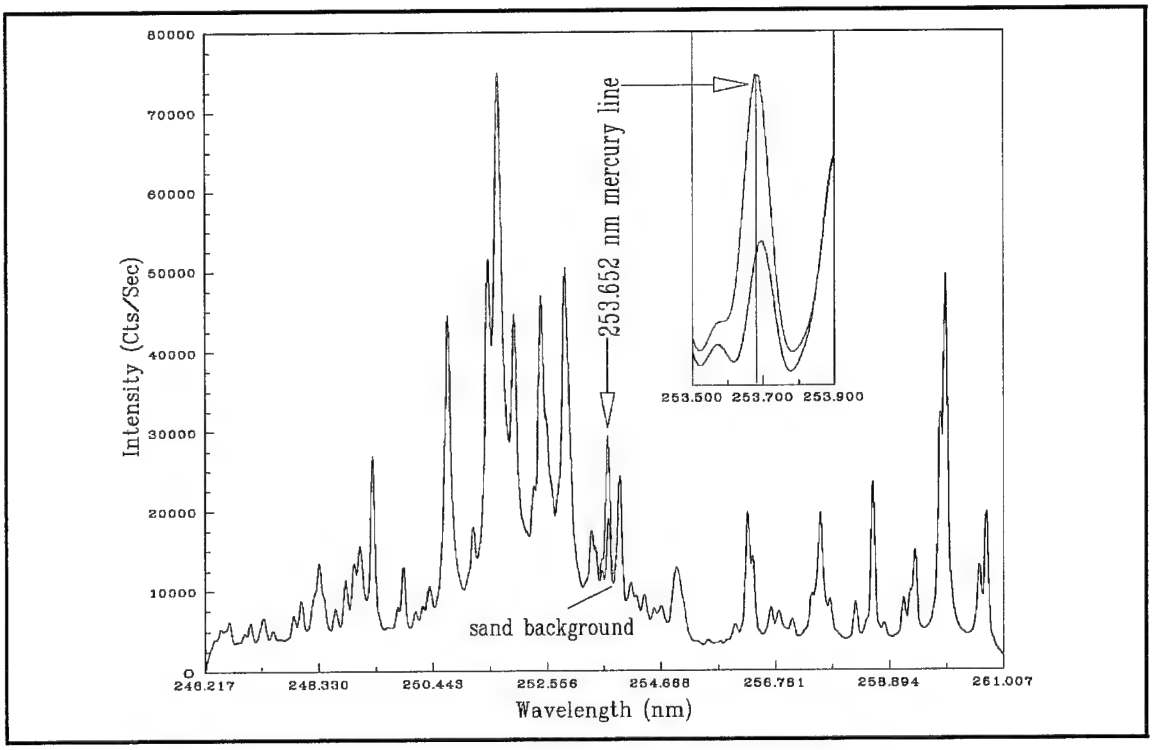

Figure 23. Spectra of 253.652-nm line of mercury at 7,800 ppm in Yuma sand

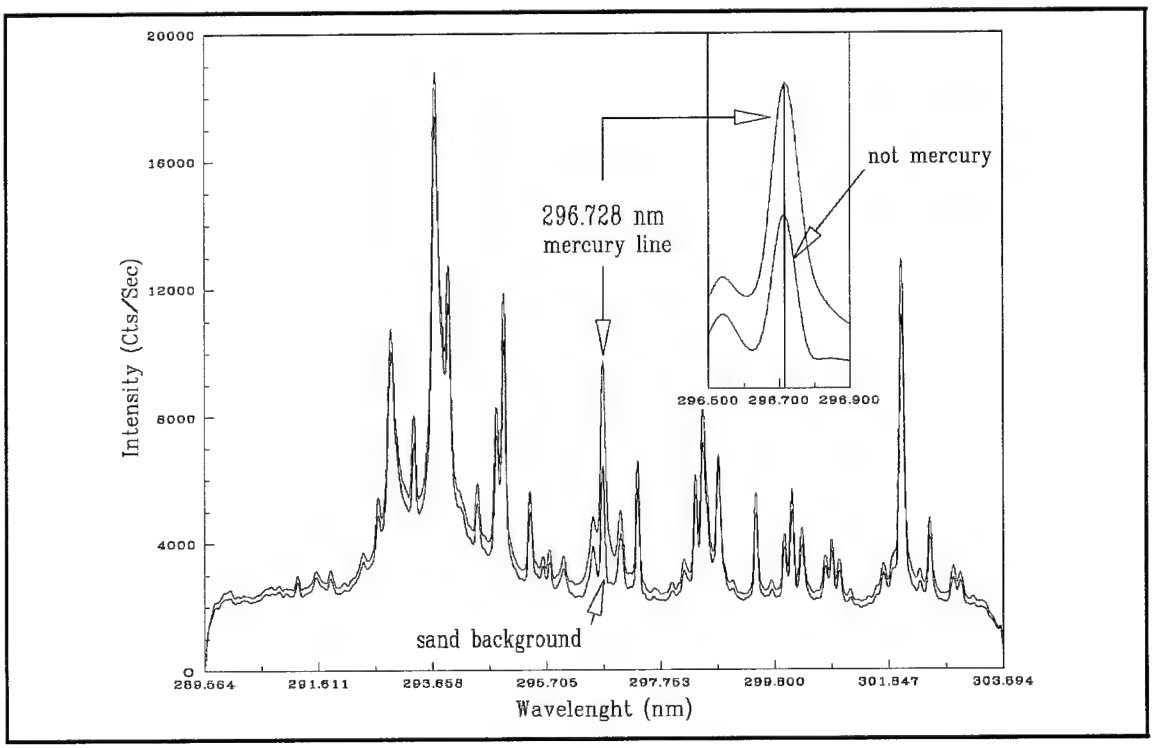

Figure 24. Spectra of 296.652-nm line of mercury at 7,800 ppm in Yuma sand

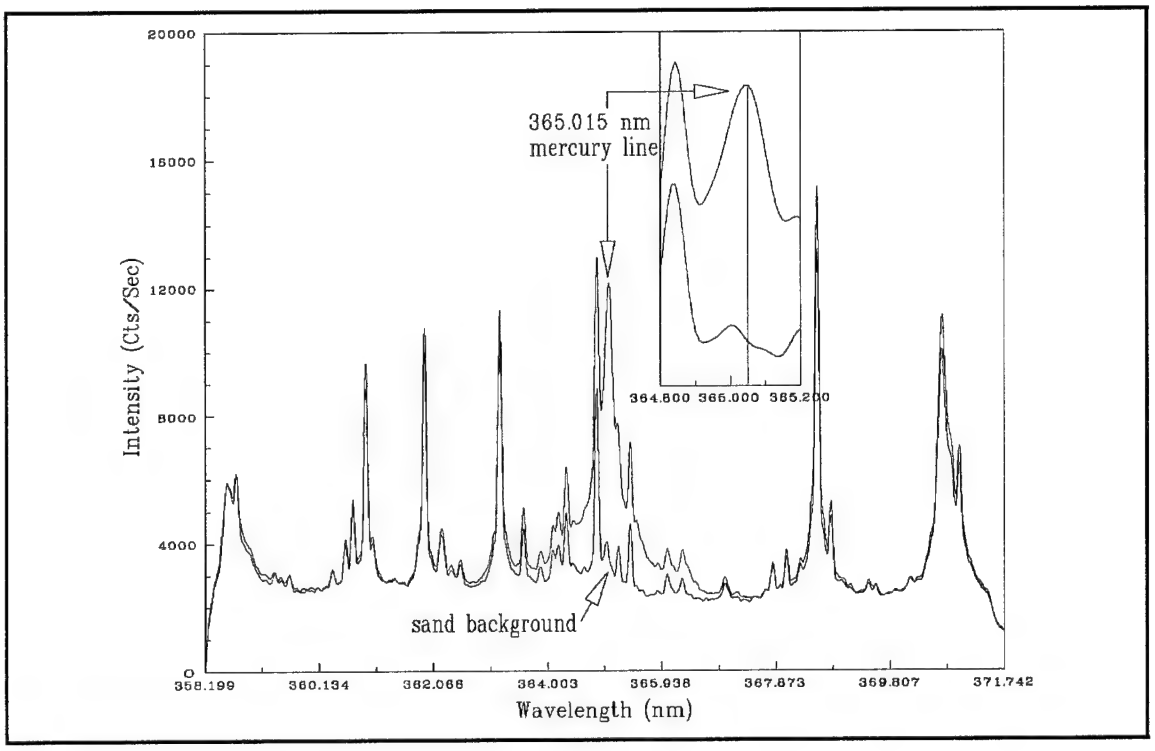

Figure 25. Spectra of 365.015-nm line of mercury at 7,800 ppm in Yuma sand

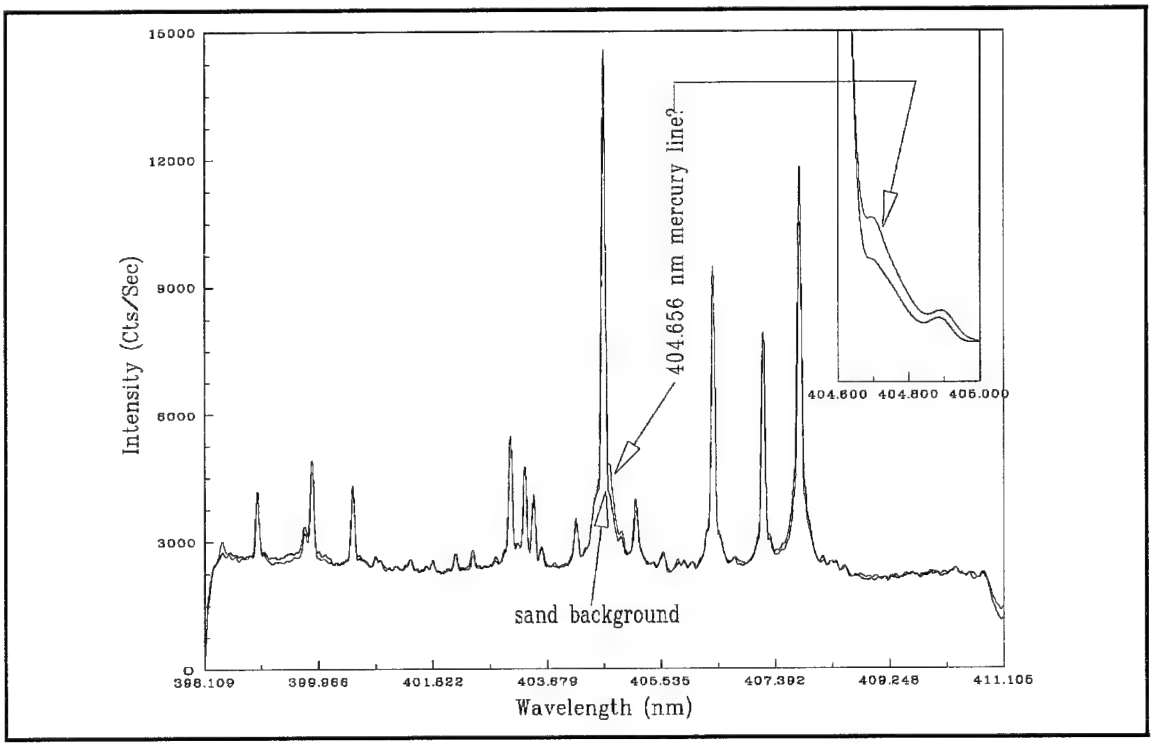

Figure 26. Spectra of 404.656-nm line of mercury at 7,800 ppm in Yuma sand

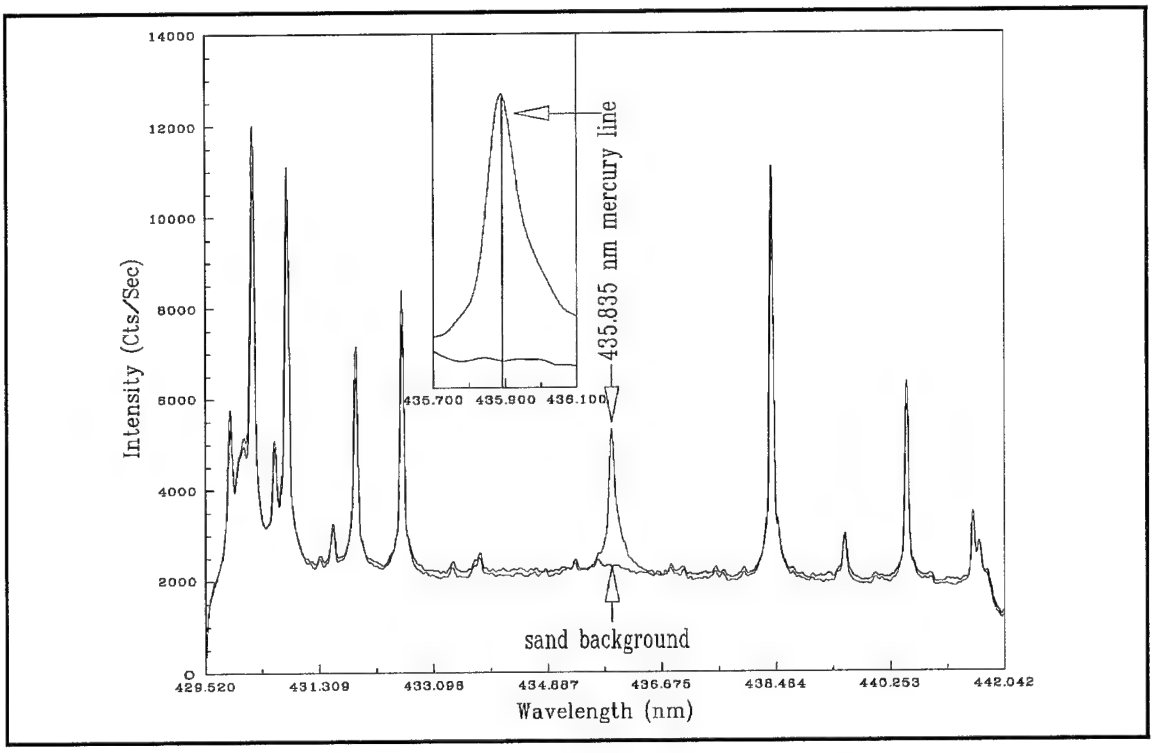

Figure 27. Spectra of 435.835-nm line of mercury at 7,800 ppm in Yuma sand

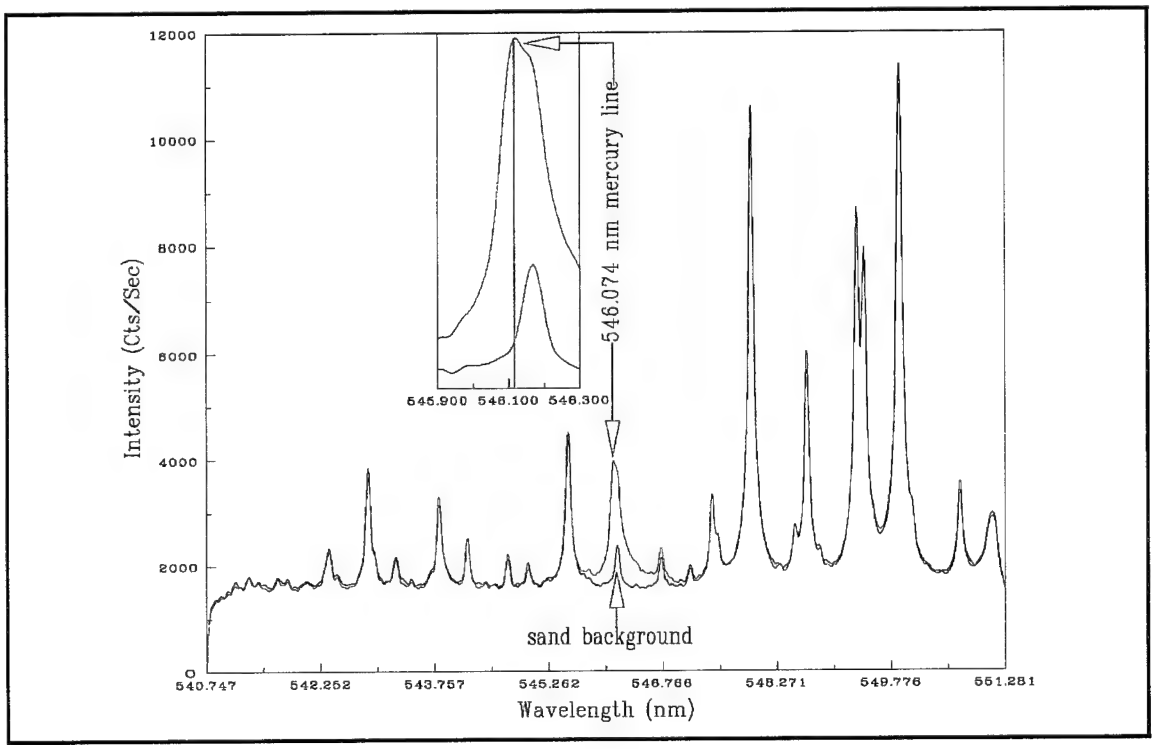

Figure 28. Spectra of 546.074-nm line of mercury at 7,800 ppm in Yuma sand

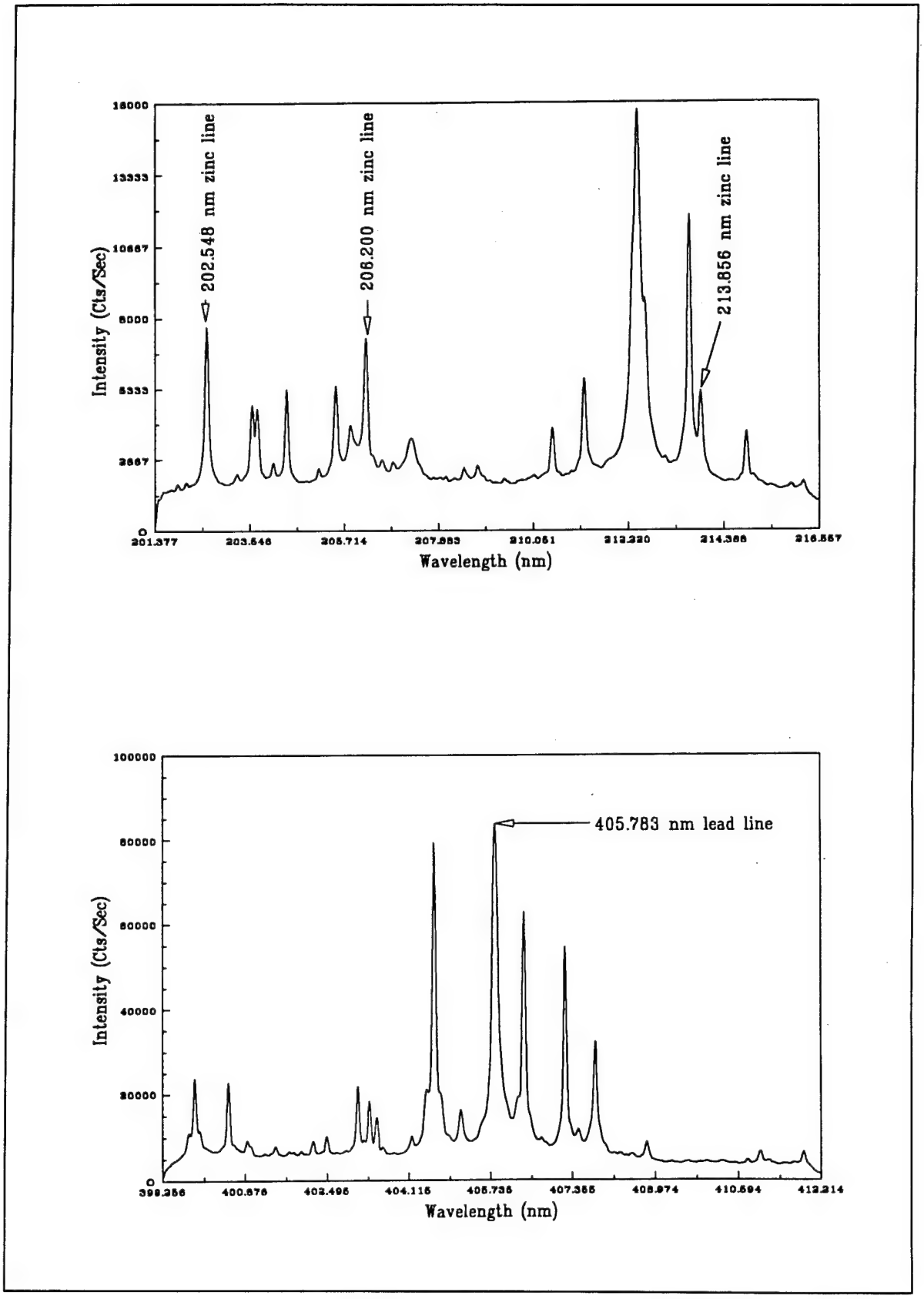

Figure 29. Spectra from samples of DoD sites contaminated with lead and zinc (Fort Ord)

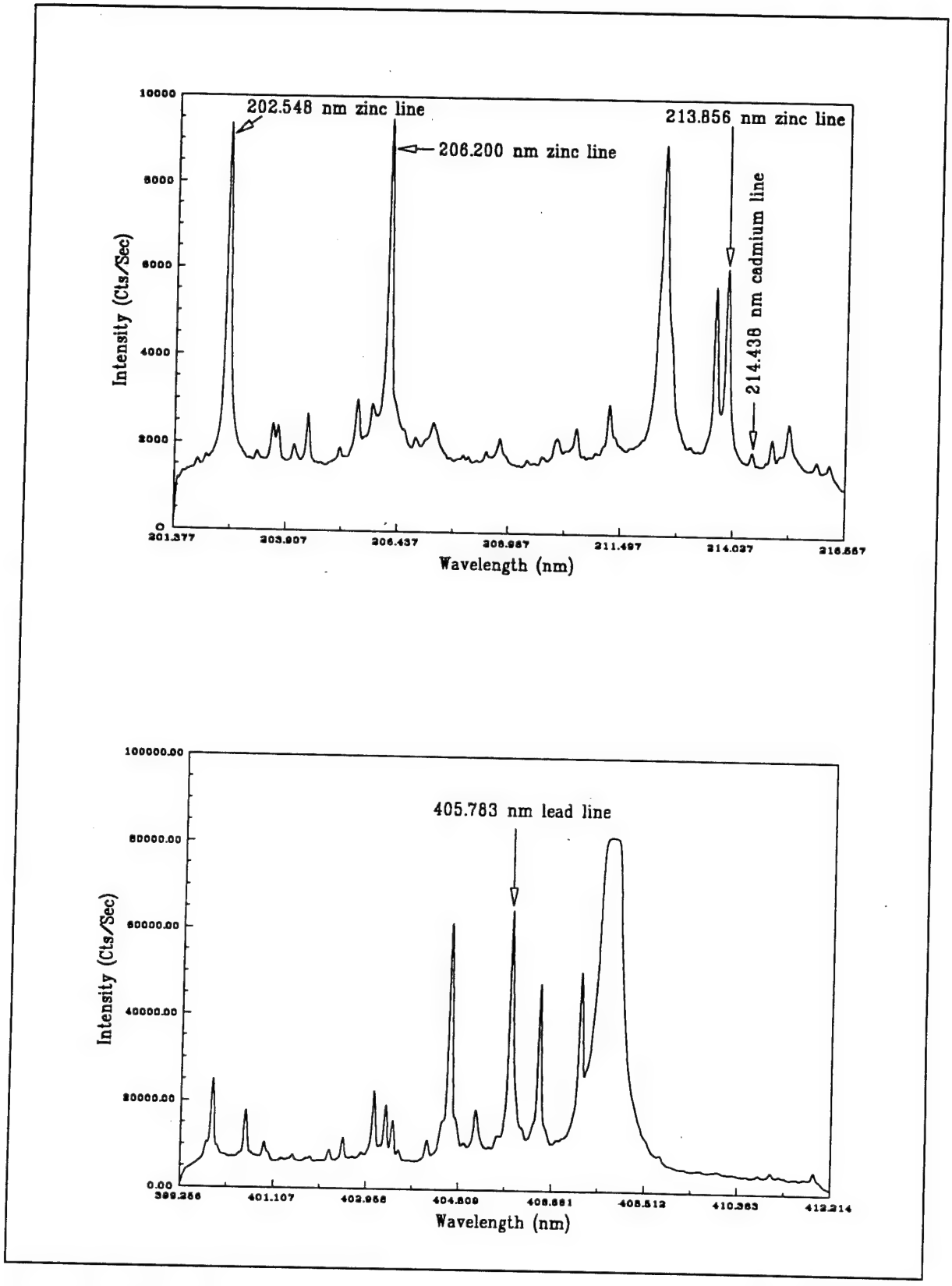

Figure 30. Spectra from samples of DoD sites contaminated with cadmium, lead, and zinc (Umatilla Army Depot)

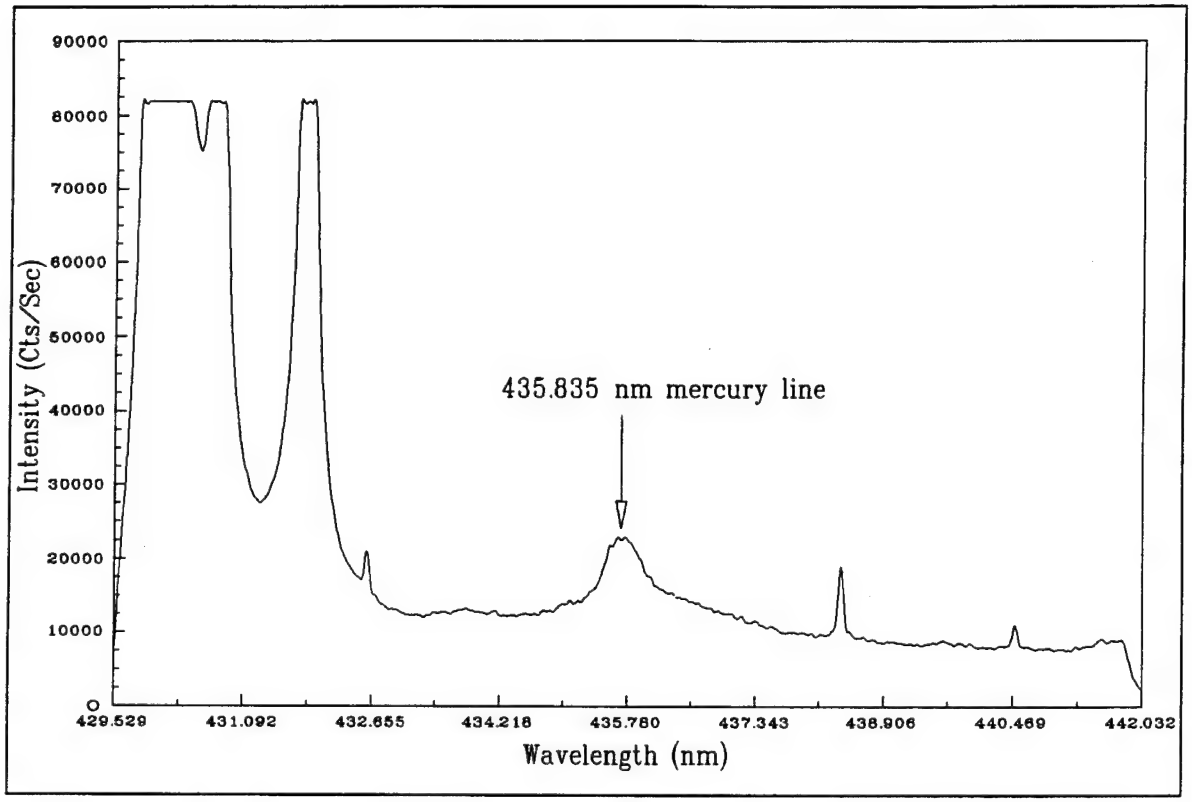

Figure 31. Spectrum from a sample of a DoD site contaminated with mercury (Rocky Mountain Arsenal)

5 New Detection Limits

After all the preliminary research described above had been completed, an optimum set of experimental parameters were established that includes the use of the 2,400-grooves/mm grating, a gate delay of 350 ns, a gate width of 100 μs, a slit opening of 10 μm, an unchanged sample height to obtain a small spot size, and a laser energy of approximately 100 mJ.

Having finally settled on a set of optimum experimental parameters, it is now possible to revisit the question of minimum detection limits for all of the metals in question in an orderly fashion. The goal is to evaluate how sensitive LIBS is for use as a screening tool in the field. Experiments were performed under the optimum laboratory conditions for lead, chromium, cadmium, mercury, and zinc in Fisher sea sand and for lead in Yuma sand to obtain the respective detection limits.

Peak Selection for Analysis of Data

As indicated earlier in this report, it was found that the best results for the detection-limits calculation were obtained by making a ratio of peak areas within the spectrum of interest.

One peak area (a measure of the area beneath a spectral line) is obviously associated with a contaminant line; the other is associated with a strong line in the soil. The reference peak and the contaminant peak have to be in the same spectral sweep (about 13 nm) to provide a picture of both peaks at the same laser energy level (remember that laser energy levels are not very stable). A large peak in the background usually represents a large concentration of a certain element, and the behavior of this peak is very repeatable in terms of the data collection, showing a constant peak area that only will depend on laser energy. The wavelengths of the contaminant and background lines used in the new detection limit calculations are shown in Table 6.

The area of a peak collected in a spectrum is observed to be a function of contaminant concentration, laser energy used to generate the plasma, gate delay, gate width, slit opening, the efficiency of the grating, and detector response. These last five parameters can be fixed in the instrumentation and

Table 6
Summary of Spectral Lines Used for Detection Limits

Heavy Metal	Soil	Heavy Metal Line Used, nm	Background Line Used, nm
lead	Yuma sand	405.785	404.576
lead	Fisher sea sand	405.785	404.576
chromium	Fisher sea sand	425.435	422.740
cadmium	Fisher sea sand	214.438	212.421
mercury	Fisher sea sand	435.835	438.429
zinc	Fisher sea sand	202.548	212.421

set to a constant value. Due to instability in the laser, the amount of energy used is a very difficult parameter to measure or to calculate. All that one can do is assume that the energy reaching the sample is a constant factor of the laser output energy. Larger contaminant concentrations will produce larger peak areas if all other conditions are fixed. As an example of how stable (or unstable) data can be for different measurement conditions, refer to Figure 32, where a limited portion of the spectra for lead-contaminated Yuma sand is shown for different contaminated levels.

Calculation of Spectral Areas

If all the instrument parameters in LIBS are fixed, the area of a peak will be a function of the contaminant concentration and laser energy used to create the plasma. If the concentration is fixed, the peak area will be only a function of laser energy; but, as mentioned before, this parameter is difficult to measure. Making a ratio of spectral areas within the range of wavelengths covered by each measurement will help to reduce the effects of shot-to-shot laser energy variations.

The most important thing in analyzing laboratory data for detection-limit calculations is the way in which the areas are selected. The method must always be consistent. After trying several approaches for data analysis, it was found that consistent results were obtained using only the peak area or a portion of the peak area and the following procedure.

A macro was written for the selection of the areas and all the mathematical manipulations. The user enters the localization of the peaks of interest for the ratio analysis. Then the macro identifies the center of the peaks and, from the center to the sides, identifies the first local minimum. These local minima serve as the reference points where the integration of the area begins and ends (see Figure 33). The macro makes the analysis for the 36 individual spectra collected and calculates the average value and the standard deviation of ratio of areas.

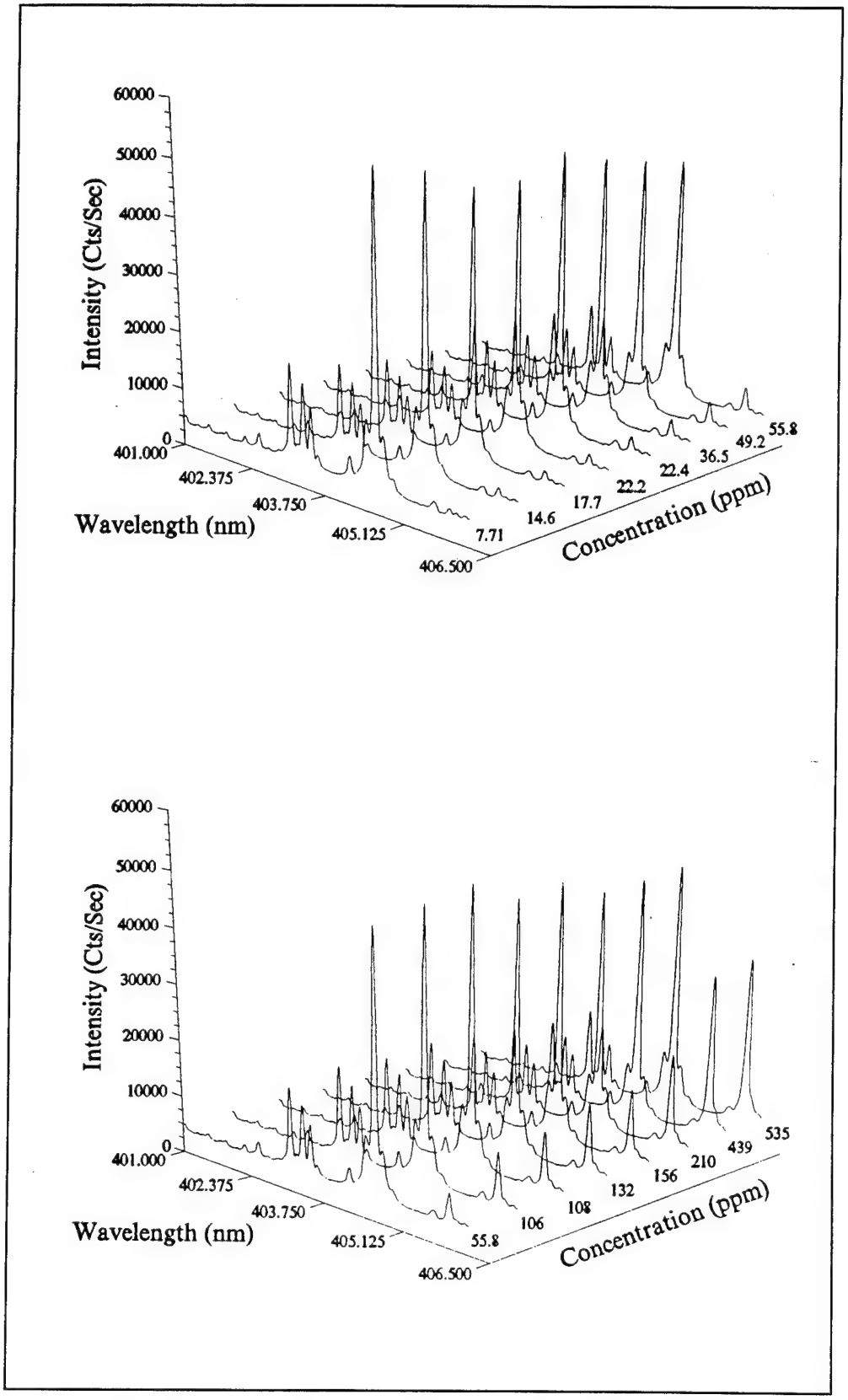

Figure 32. Spectra of 405.783-nm lead line in Yuma sand (Concentration increasing into the page)

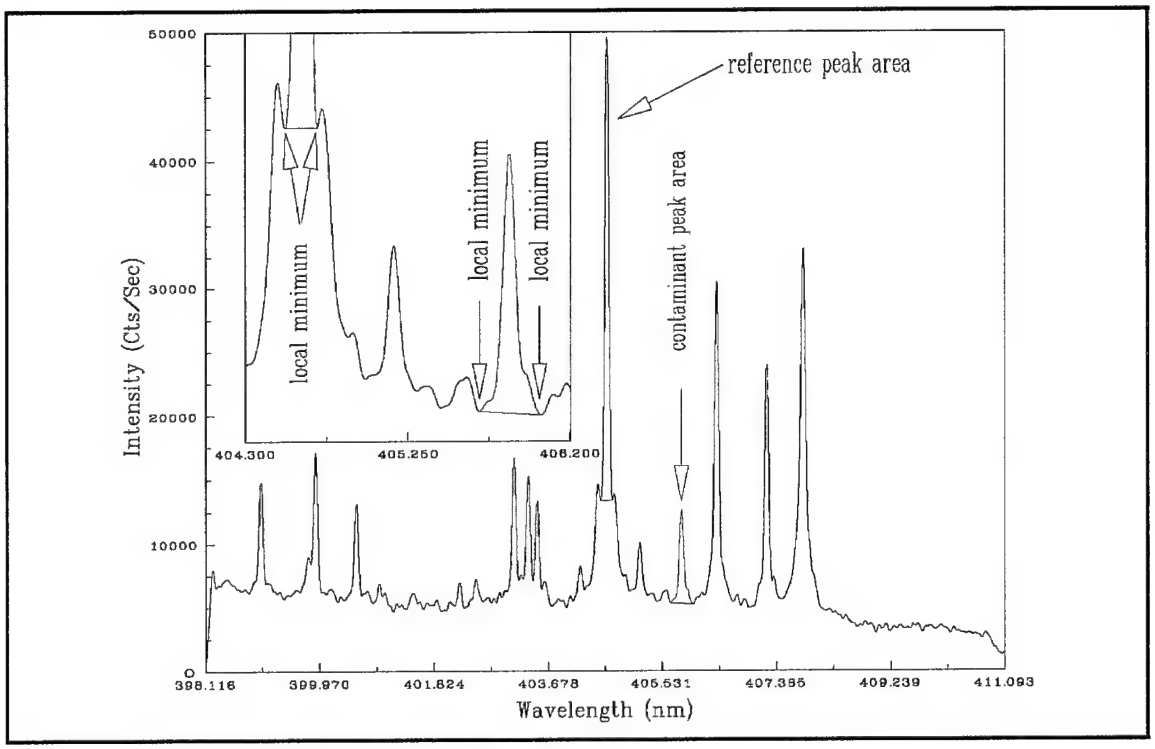

Figure 33. Example of detection-limit analysis for Yuma sand contaminated with 108 ppm of lead

where the standard deviation of the ratio of areas is obtained from the macro for each sample. A plot of the average ratio versus concentration is generated to obtain the slope of the calibration curve (see Figures 34-39).

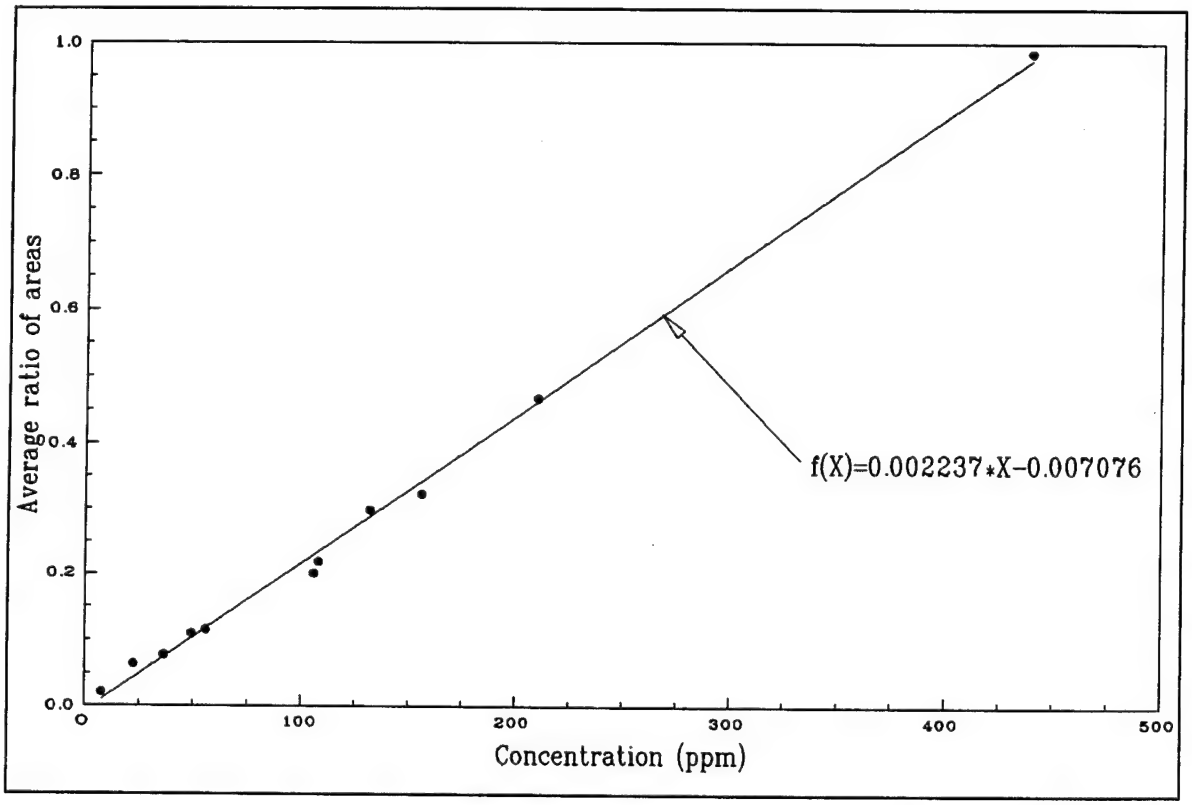

Figure 34. Calibration curve for detection-limit calculation of lead in Yuma sand at laser energy of 100 mJ

An example of a detection-limit calculation for lead in Yuma sand is:

$$C_L = \frac{Z^* S_B}{M}$$

C_L = 9.14 ppm of lead in Yuma sand

Z = 2

S_B = 0.010224

M = 0.002237/ppm

A summary of the detection limits for each metal in sands using this methodology is shown in Table 7. Following the summary table, spectra are shown for each set of experiments (Figures 40-45). The contaminant line is blown up to show the lowest measured response.

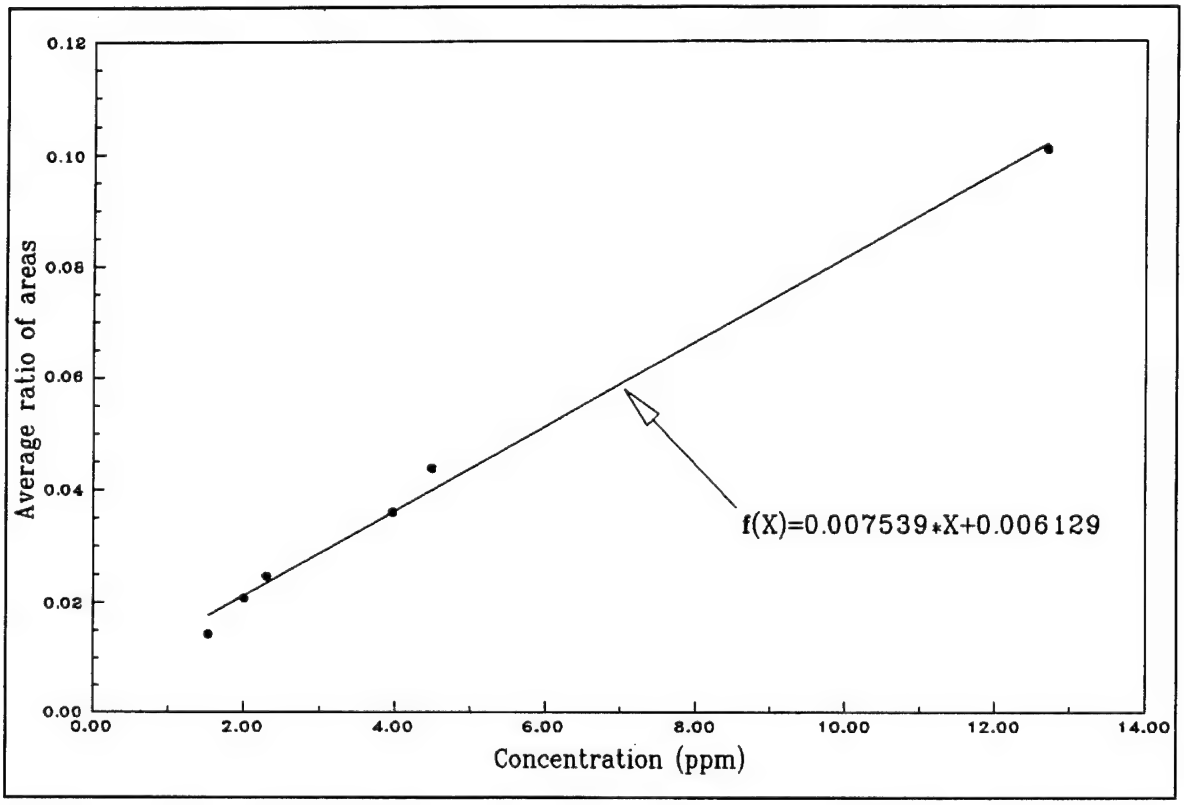

Figure 35. Calibration curve for detection-limit calculation of lead in Fisher sea sand at laser energy of 100 mJ

Particular attention should be given to Figure 44, which shows the 435-nm Hg line in Fisher sea sand. In Chapter 4, Figure 31, LIBS data for the same line were shown for a sediment collected at the Rocky Mountain Arsenal. Note that the background peaks for these two spectra are entirely different, clearly demonstrating that different soils provide different responses.

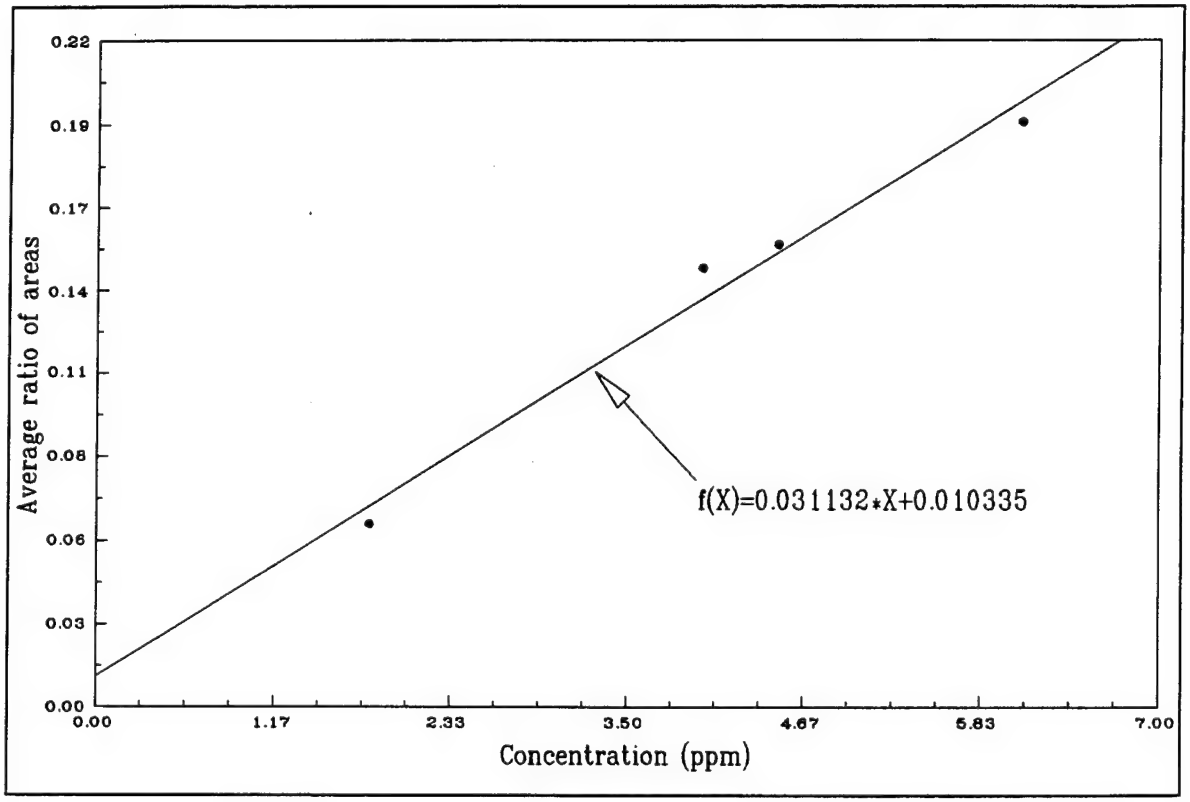

Figure 36. Calibration curve for detection-limit calculation of chromium in Fisher sea sand at laser energy of 100 mJ

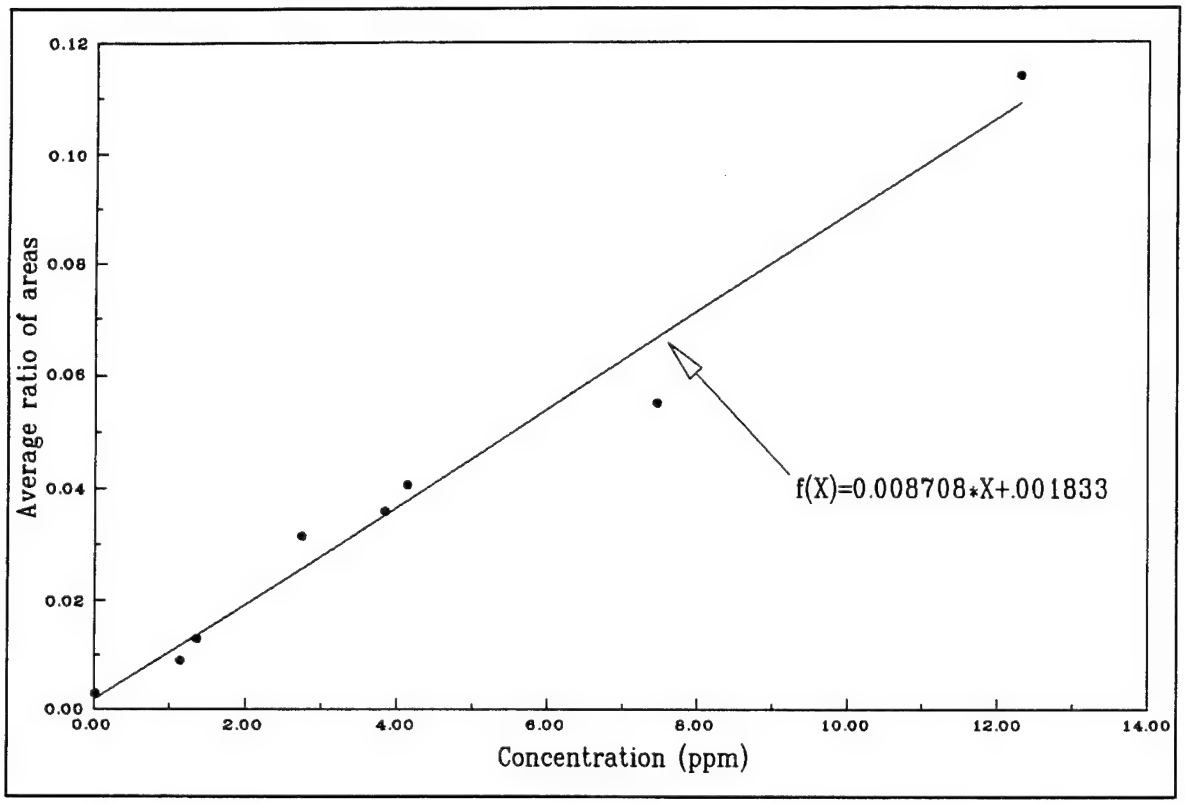

Figure 37. Calibration curve for detection-limit calculation of cadmium in Fisher sea sand at laser energy of 100 mJ

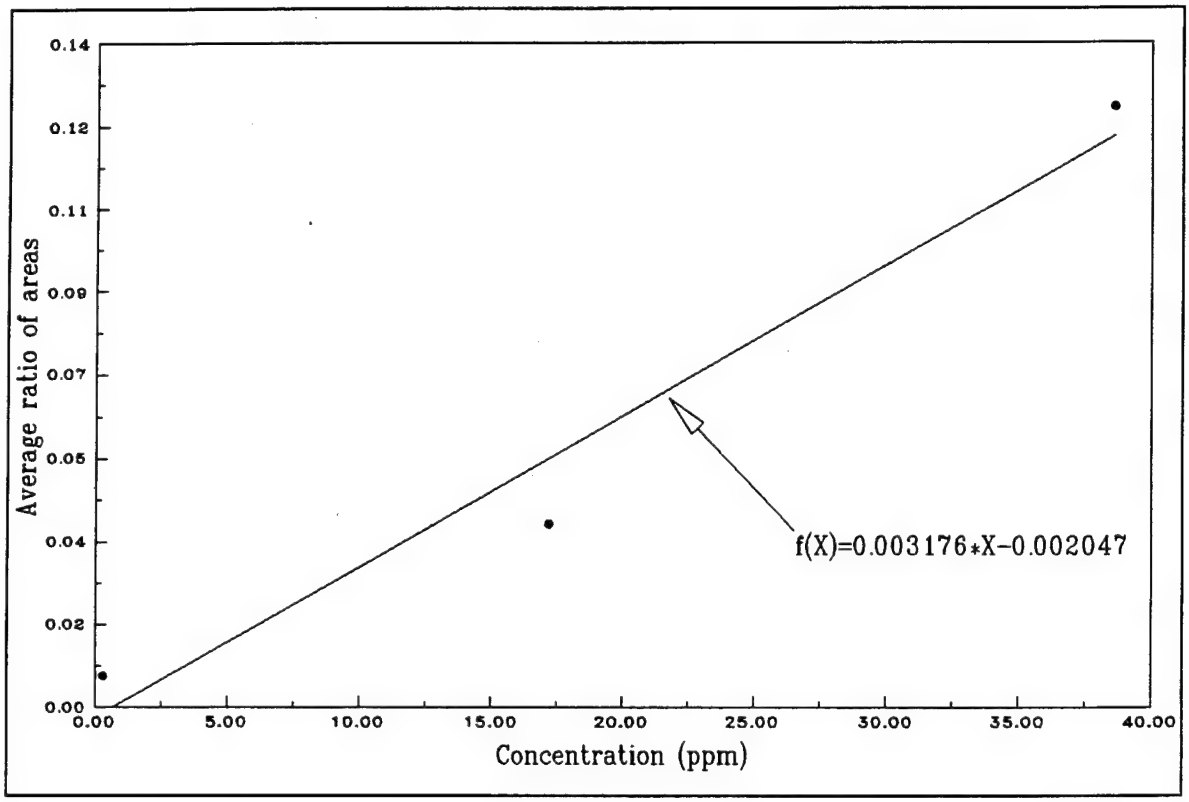

Figure 38. Calibration curve for detection-limit calculation of mercury in Fisher sea sand at laser energy of 100 mJ

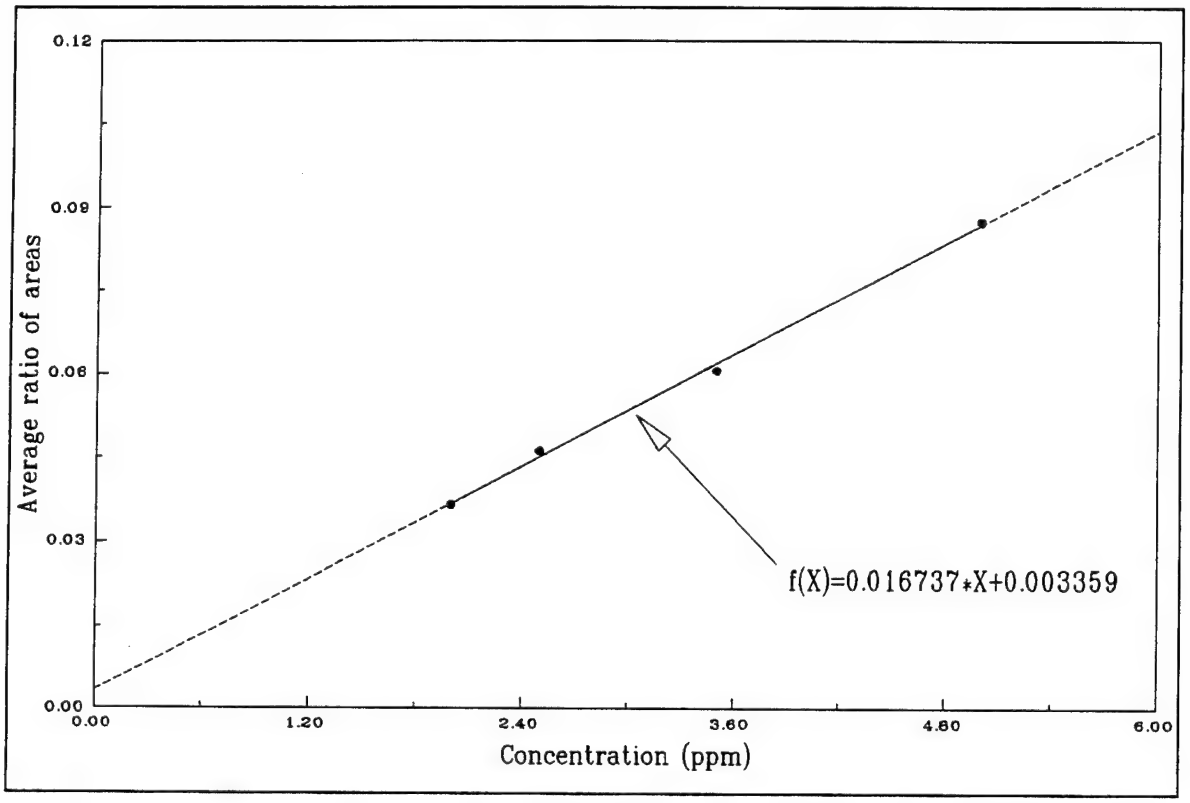

Figure 39. Calibration curve for detection-limit calculation of zinc in Fisher sea sand at laser energy of 100 mJ

Table 7
Summary of Detection Limits

Heavy Metal	Soil	Lowest Concentration Used (u) or Detected (d), ppm	Detection Limit ppm
lead	Yuma sand	7.71 (u)	9.14
lead	Fisher sea sand	2.00 (d)	3.32
chromium	Fisher sea sand	1.80 (d)	1.62
cadmium	Fisher sea sand	1.14 (d)	1.10
mercury	Fisher sea sand	17.2 (u)	3.77
zinc	Fisher sea sand	1.30 (d)	0.99

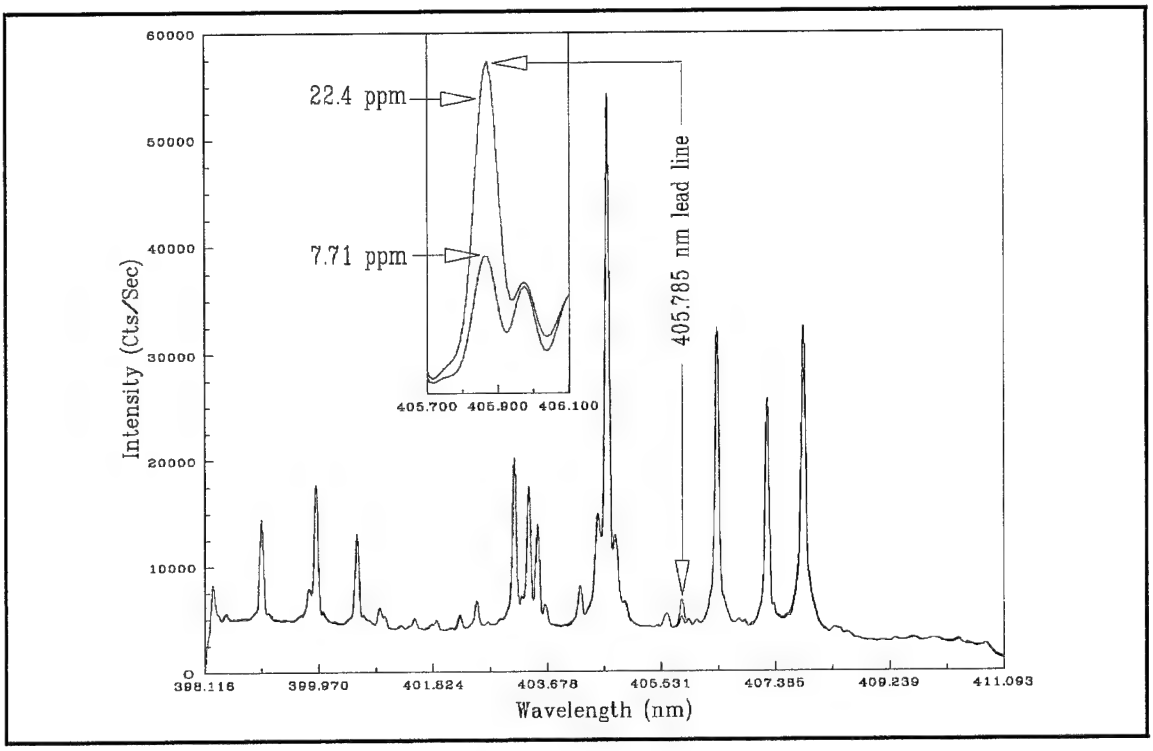

Figure 40. Spectra of Yuma sand and 405.785-nm lead line at 7.71 and 22.4 ppm

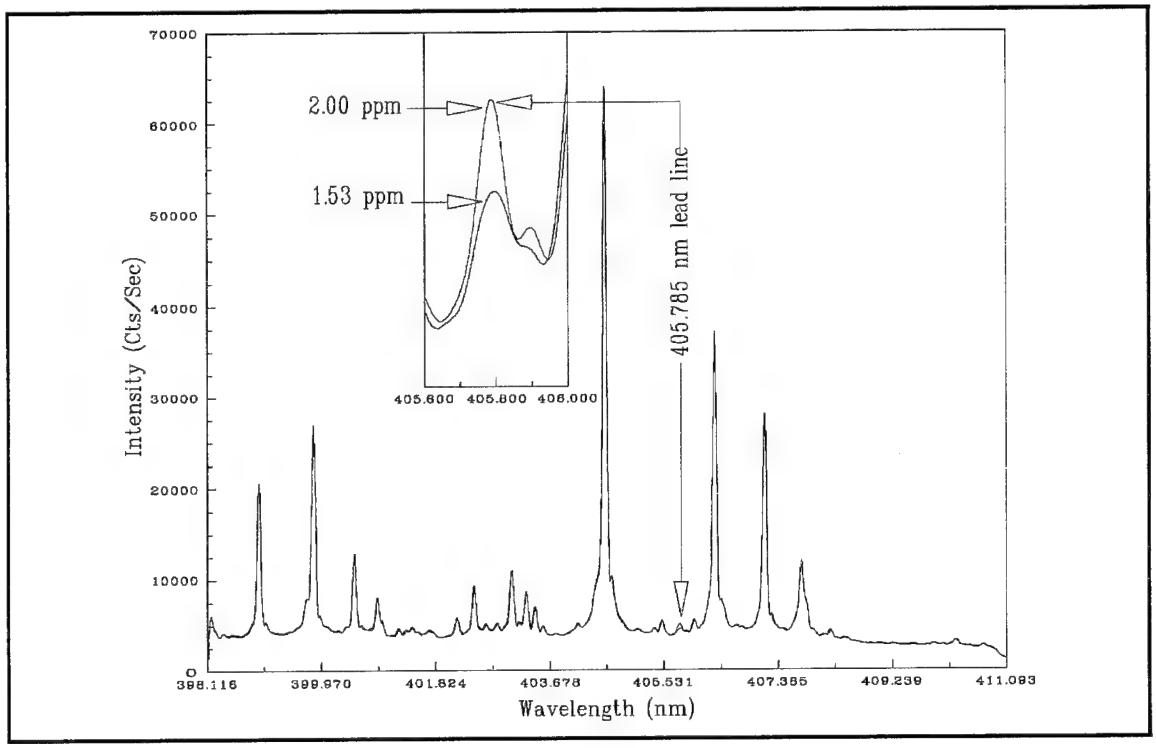

Figure 41. Spectra of Fisher sea sand and 405.785-nm lead line at 1.53 and 2.00 ppm

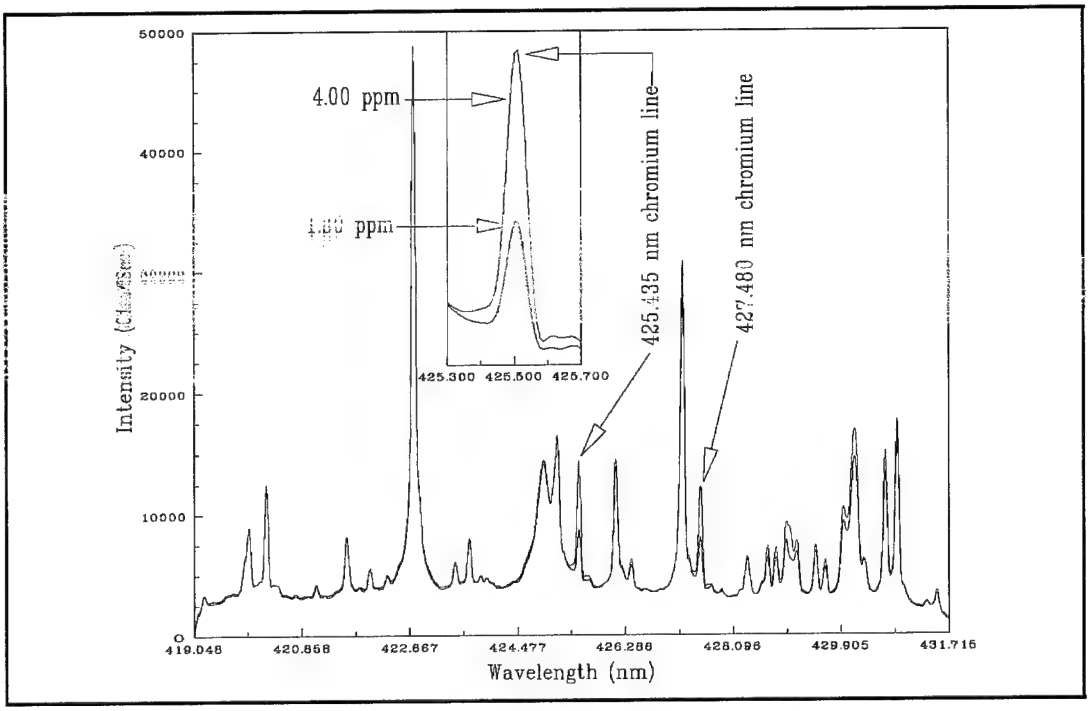

Figure 42. Spectra of Fisher sea sand and 425.435-nm chromium line at 1.80 and 4.0 ppm

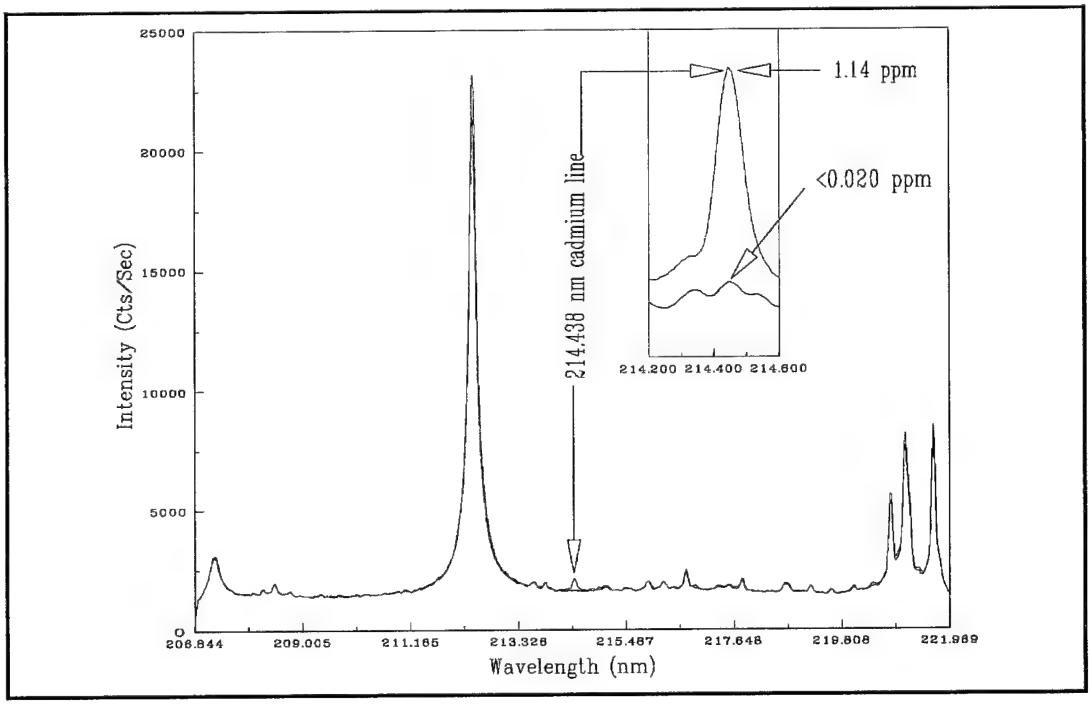

Figure 43. Spectra of FIsher sea sand and 214.438-nm cadmium line at 1.14 ppm

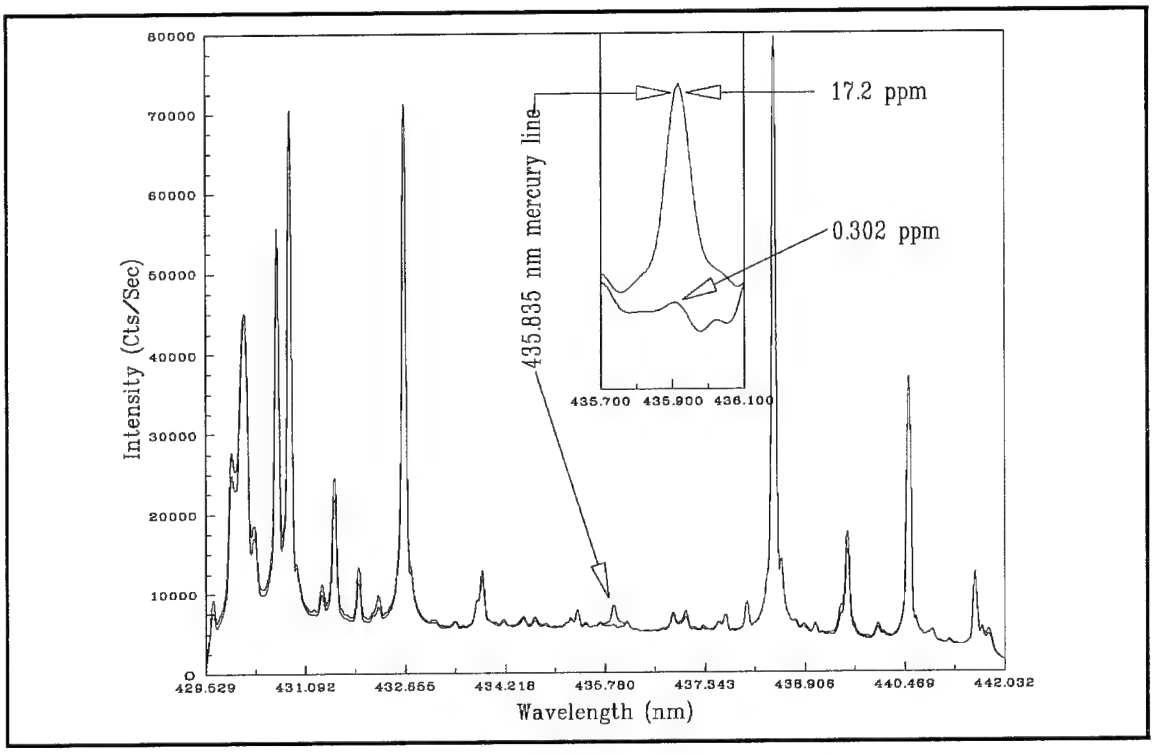

Figure 44. Spectra of Fisher sea sand and 435.835-nm mercury line at 17.2 ppm

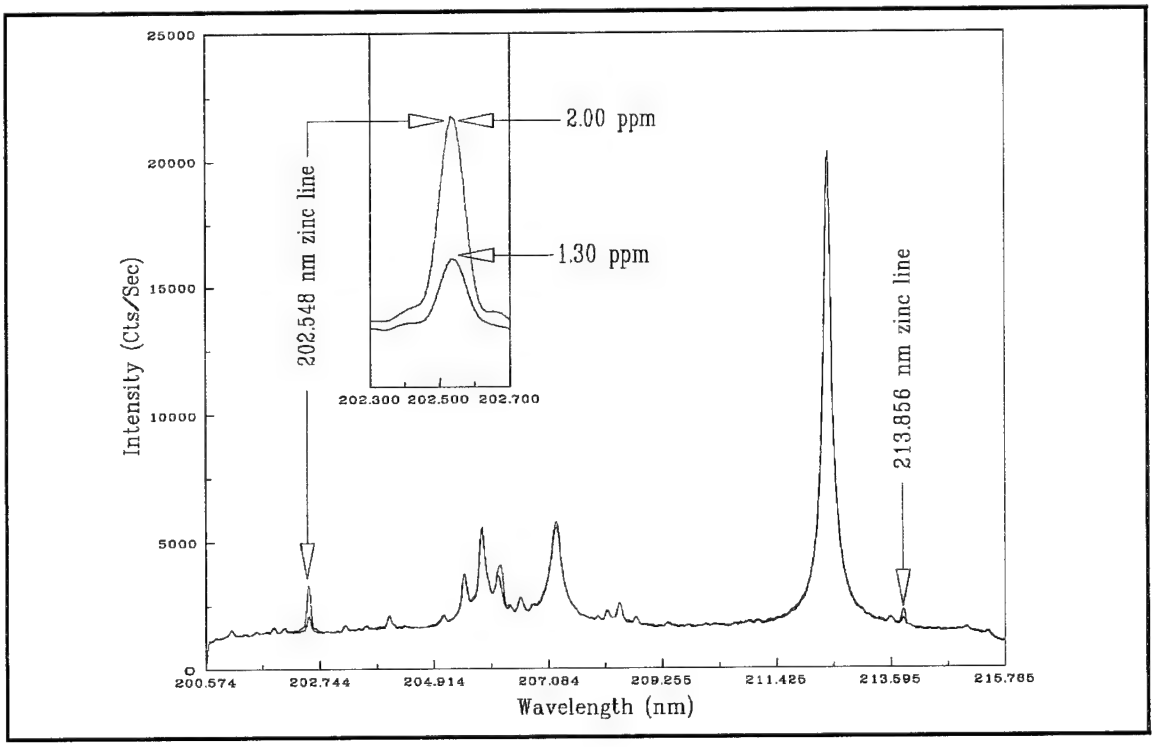

Figure 45. Spectra of Fisher sea sand and 202.548-nm line at 1.30 and 2.00 ppm

6 Conclusions

The LIBS technique and instrumentation currently has the potential to be a very effective sensor for detection of heavy metals in soil. LIBS has been demonstrated to be a powerful tool in the detection of the heavy metals. The technique has detection limits as low as 1.10 ppm for cadmium, 0.99 ppm for zinc, 1.62 ppm for chromium, 3.32 ppm for lead, and 3.77 ppm for mercury in sea sand bought from the Fisher Company. These low concentrations of contaminants were detected at wavelengths of 214.438 nm for cadmium, 202.548 nm for zinc, 425.435 nm for chromium, 405.785 nm for lead, and 435.835 nm for mercury. LIBS has the capability of making elemental analysis of soils in real-time. The implementation of LIBS into a cone-penetrometer geometry (such as SCAPS) would allow for in situ elemental analysis of the soil matrix and inorganic gases and would give SCAPS one of the most powerful sensors for the detection of contaminants in soils.

Emphasis is now shifting toward fabricating a prototype sensor for the SCAPS truck. It is expected to obtain from this sensor detection limits of heavy metals below the 10 ppm for sands, below the 20 ppm for silts, and below the 35 ppm for clays.

As with any intensive research effort, several questions were answered, and several more were generated. More work needs to done in other soils to investigate their backgrounds and how contaminants will appear in those matrices. More research of contaminant emission lines in the visible region needs to be done for the detection of these in the soils. Work needs to be done in increasing the signal of the contaminant peak from the background interference, perhaps by changing the time parameters of the data collection.

Future research should also continue to focus on the quantification of LIBS. For example, can the issue of shot-to-shot laser energy variations be incorporated into a meaningful model? Some preliminary data have been collected in this regard and are shown in Figure 46. These data represent the behavior of lead in Yuma sand at different laser energy levels and concentrations. The LIBS sensitivity can possibly be increased from low parts per billion to hundreds of parts per billion by using higher laser energy levels and more data points per data set.

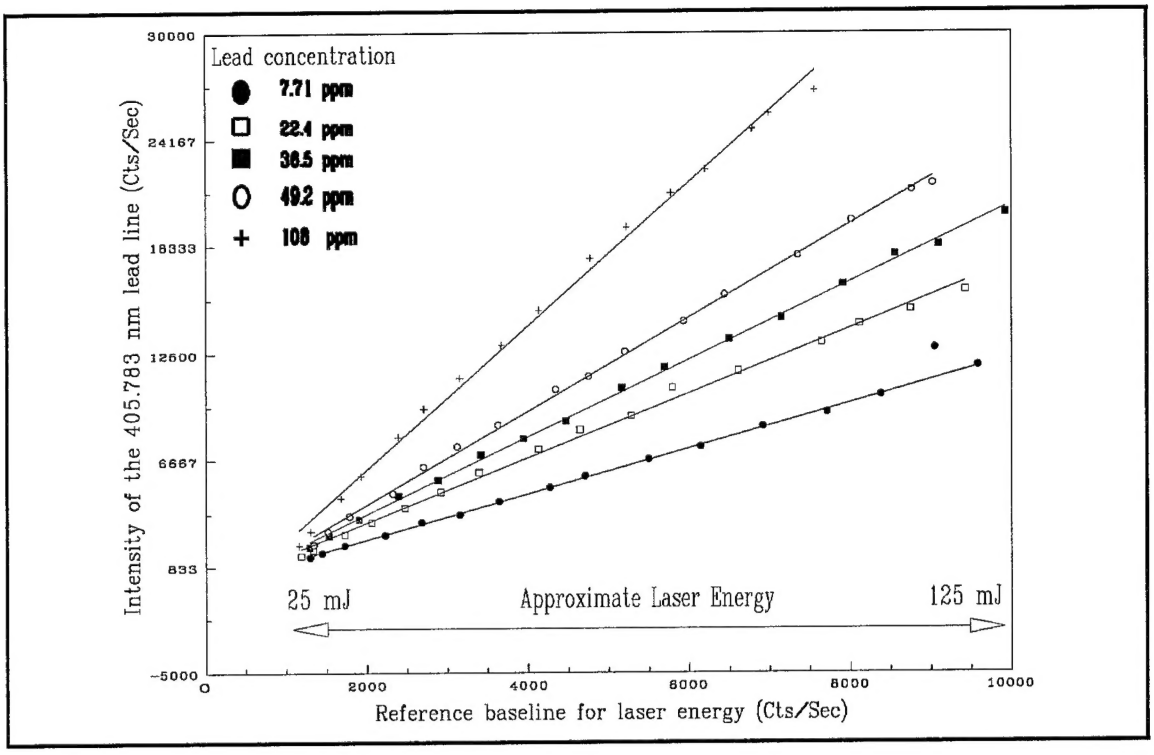

Figure 46. Preliminary results of quantification of LIBS data (Lead in Yuma sand)

References

Alexander, D. R., Poulain, D. E., Schaub, S. A., and Barton, J. P. "Laser-induced breakdown spectroscopy method for measuring salt concentration in sprays."

Cespedes, E. R., Miles, B. H., and Lieberman S. H. (1994). "Development of optical sensors for the site characterization and analysis penetrometer system (SCAPS)," Optical Sensing for Environmental Monitoring, Air and Waste Management Assoc., Pittsburgh, PA.

Fritz, J. S., and Schenk, G. H. (1987). *Quantitative analytical chemistry*. 5th ed., Chapter 19, Allyn and Bacon, Inc., Boston, MA.

Meggers, W. F., Corliss, C. H., and Scribner, B. F. (1975). "Tables of spectral-line intensities," NBS monograph 145, U.S. Department of Commerce/National Bureau of Standards, Washington, DC.

Robinson, J. W. (1991). *Practical handbook of spectroscopy*. 1st ed., CRC Press, Inc., Boca Raton, FL.

Weyl, G. M. (1989). "Chapter 1, Physics of laser-induced breakdown: An update." *Laser-induced plasmas and applications*. Leon J. Radziemski and David A. Cremers, ed., Marcel Dekker, Inc., New York.

REPORT DOCUMENTATION PAGE

Form Approved
OMB No. 0704-0188

1. AGENCY USE ONLY *(Leave blank)*	2. REPORT DATE	3. REPORT TYPE AND DATES COVERED
	March 1996	Final report

4. TITLE AND SUBTITLE
Development of Laser-Induced Breakdown Spectroscopy for Detection of Metal Contaminants in Soils

5. FUNDING NUMBERS

6. AUTHOR(S)
Javier Cortes, Ernesto R. Cespedes, Brian H. Miles

7. PERFORMING ORGANIZATION NAME(S) AND ADDRESS(ES)
U.S. Army Engineer Waterways Experiment Station
3909 Halls Ferry Road, Vicksburg, MS 39180-6199

8. PERFORMING ORGANIZATION REPORT NUMBER
Technical Report
IRRP-96-4

9. SPONSORING/MONITORING AGENCY NAME(S) AND ADDRESS(ES)
U.S. Army Corps of Engineers
Washington, DC 20314-1000

10. SPONSORING/MONITORING AGENCY REPORT NUMBER

11. SUPPLEMENTARY NOTES
Available from National Technical Information Service, 5285 Port Royal Road, Springfield, VA 22161.

12a. DISTRIBUTION/AVAILABILITY STATEMENT
Approved for public release; distribution is unlimited.

12b. DISTRIBUTION CODE

13. ABSTRACT *(Maximum 200 words)*

This technical report covers 3 years of research done in Laser-Induced Breakdown Spectroscopy (LIBS) at the U.S. Army Engineer Waterways Experiment Station by the Environmental Sensing Branch (ESB). LIBS was used and evaluated as a sensing technique for detection of heavy metal contaminants in soils. The primary heavy metals studied were lead, chromium, cadmium, mercury, and zinc in soils. Topics addressed in the report include detection limits for these metals in sand, experimental setup, experimental considerations, and many observations of the plasma behavior under laboratory conditions. Conducted as an effort of ESB to provide new technology for detection of environmental contaminants, LIBS has demonstrated potential as a very effective sensor. LIBS is expected to be used as a screening sensor and interface with the Site Characterization and Analysis Penetrometer System truck.

14. SUBJECT TERMS		15. NUMBER OF PAGES
Contaminated soils	Laser-induced breakdown spectroscopy (LIBS)	72
Heavy metals	Metals contamination	16. PRICE CODE

17. SECURITY CLASSIFICATION OF REPORT	18. SECURITY CLASSIFICATION OF THIS PAGE	19. SECURITY CLASSIFICATION OF ABSTRACT	20. LIMITATION OF ABSTRACT
UNCLASSIFIED	UNCLASSIFIED		